Heliyon 9 (2023) e19965

Contents lists available at ScienceDirect

Heliyon

journal homepage: www.cell.com/heliyon

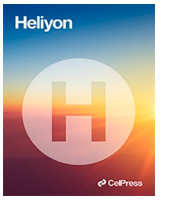

Structural, electronic, intermolecular interaction, reactivity, vibrational spectroscopy, charge transfer, Hirshfeld surface analysis, pharmacological and hydropathy plot on 5-Bromo nicotinic acid – Antiviral study (Hepatitis A, B, and C)

Sravanthi R [a,b], S. Mahalakshmi [a], S. Kumaran [c], Shine Kadaikunnan [d], Ghulam Abbas [e], S. Muthu [f,*]

[a] Department of Physics, Ethiraj College for Women, Chennai, 600008, Tamil Nadu, India
[b] University of Madras, Chennai, 600005, Tamil Nadu, India
[c] Department of ECE, Saveetha Engineering College, Thandalam, Chennai, 602105, Tamil Nadu, India
[d] Department of Botany and Microbiology, College of Science, King Saud University, P.O. Box 2455, Riyadh 11451, Saudi Arabia
[e] Institute of Inorganic Chemistry, Karlsruhe Institute of Technology, Engesserstr 15, 76131, Karlsruhe, Germany
[f] Department of Physics, Arignar Anna Govt. Arts College, Cheyyar, 604407, Tamil Nadu, India

ARTICLE INFO

Keywords:
DFT
NBO
Hirshfeld
Molecular docking
ELF

ABSTRACT

The therapeutic properties of 5-Bromonicotinatic acid (5BNA) were studied for antiviral illnesses like Hepatitis A, Hepatitis B and Hepatitis C and the influence of electron-donating and electron-withdrawing properties of functional groups on the nicotinic acid was evaluated and represented in this study using the DFT approach. The molecular parameters were determined for both gases as well as for various solvent phases. The reactive areas in the compound are examined utilising Fukui analysis. The molecular interactions are accomplished by recognising the different types of bonding found in the compound using the AIM, ELF, LOL, RDG and IRI. Solvation investigations were demonstrated to have an influence on molecular orbital energy, ESP, UV–Vis and NLO analyses. Electron-hole, NBO and Hirshfeld investigations are used to investigate the transfer of charges and interactions inside the molecule. The method of vibrational spectroscopy (IR and Raman) is used to differentiate and identify the various types of vibrations displayed by the compound. The hydropathy plots for the proteins 2A4O, 6CWD and 2OC8 associated with Hepatitis A, Hepatitis B and Hepatitis C illustrate the disquiet and attraction of the amino acids towards the water.

1. Introduction

Pyridine is the fundamental aromatic and heterocyclic organic compound. It shares a structural resemblance with benzene but has a nitrogen atom in place of one of the methyl groups [1]. It is a colourless compound with high conductivity of electricity and is used in various branches of chemistry, including catalytic reactions, clinical trials, identification of molecules, etc. Pyridine has been found to be a major constituent in numerous naturally occurring substances that are significant to biological sciences. The prevalence of

* Corresponding author.
E-mail address: mutgee@gmail.com (S. Muthu).

https://doi.org/10.1016/j.heliyon.2023.e19965
Received 28 July 2023; Received in revised form 22 August 2023; Accepted 7 September 2023
Available online 7 September 2023

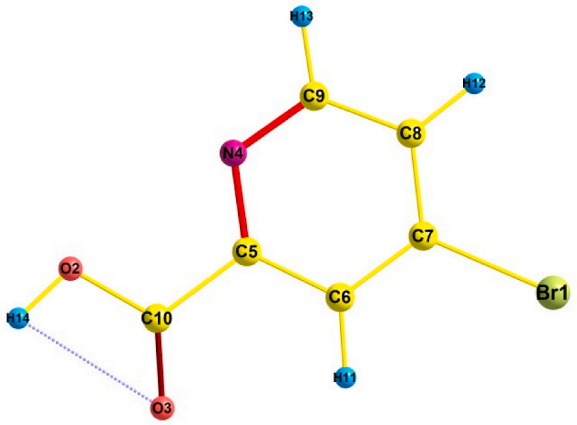

Fig. 1. Optimised structure of 5BNA.

pyridines in a wide range of natural chemicals and pharmaceuticals, as well as their powerful bioactivities, has piqued the pharmaceutical sector's attention [2]. Pyridine derivatives are important because of their sedative and hypnotic effects. They are available in naturally occurring products such as vitamin B and also have a variety of therapeutic effects in living systems, such as antimicrobial, anti-inflammatory, antiviral, antitumour, etc [3].

Niacin, also known as nicotinic acid, is a pyridine derivative and a particular form of vitamin complex, which is essential for human health [4]. Living organisms such as plants and animals can provide it naturally from tryptophan (amino acid). Nicotinic acid is utilised in medical therapies such as maintaining blood levels of triglycerides and cholesterol, treatment of vitamin B deficiency such as pellagra and boosting lipid and protein metabolism [5]. Nicotinamide is the derivative of nicotinic acid and it is used as a core component in the production of enzymes such as NAD (Nicotinamide Adenine Dinucleotide) and NADP (Nicotinamide Adenine Dinucleotide Phosphate) [6].

5-Bromonicotinic acid (5BNA) is one of the derivatives of nicotinic acid containing the halogen bromine in it [7]. It has a molecular formula of $C_6H_4BrNO_2$ and a mass of 202.01 u and has been selected for quantum chemical investigation. A computational technique emphasised by Density Functional Theory (DFT) is used to determine the physiochemical properties of 5BNA. A comprehensive study of the literature revealed that the computational assessment of the molecule in question has not yet been done, so we studied it using DFT calculations [8]. The structural conformation, morphological, dynamics, and electronic characteristics of the heading molecule have all been thoroughly computed. The title compound is studied using solvents such as water, chloroform, diethyl ether and acetonitrile [9]. To differentiate and specify various functional groups that are present in organic molecules, vibrational spectroscopy is employed. The reactive areas are examined through ESP and Fukui and the chemical bonding of the molecule is examined through ELF (electron localization function) and LOL (localised orbital locator). NBO (natural bond orbital) analysis is employed to identify the charge transfer and the stability, while NLO (nonlinear optics) is used to evaluate the compound's optical activity. AIM (Atoms in molecules), RDG (Reduced density gradient), IRI (Interaction region indicator) and VdW are employed to characterize interactions [10]. Electron - Hole and Hirshfeld analysis is used to investigate charge transport and intramolecular interaction. Docking studies establish physiological characteristics and features for toxicity and drug-likeness have also been accomplished [11].

2. Methodology

The quantum chemistry calculation was carried out using the DFT package of the Gaussian 09 and Gauss View 06 applications [12, 13]. The conventional 6-311-G ++(d,p) basis was chosen in this work due to being the higher basis in the B3LYP approach and it offers superior precision for computations in both the ground and excited states. The TD-DFT technique is used in UV–Vis analysis. The vibrational assignments for the heading compound are determined using the VEDA [14] programme. The topographical parameters as well as the non-covalent interactions are computed by Multiwfn 3.7 [15]. The SWISSADME [16], Gusar [17] and ProTox-II [18] tools are utilised for the physiological analysis of the molecule, which is easily accessible online. PyRx [19] is utilised for molecular docking and Biovia Discovery Studio [20] for visual representation.

3. Results and discussions

3.1. Structure analysis

The 5BNA is computationally optimised as shown in Fig. 1 [21] and Table S1 gives the bond characteristics of its gaseous form as well as in different solvents. The XRD results of the 5BNA show that it has a triclinic structure with intercepts of 8.2576 Å, 11.0316 Å and 17.648 Å and has angles 93.9010°, 95.644° and 91.486° [22]. There is one Br–C bond, two O–C bonds, two N–C bonds, two O–H bonds, three C–H bonds, and five C–C bonds in this compound. The highest bond length is observed at O3–H14 and Br1–C7. The bond

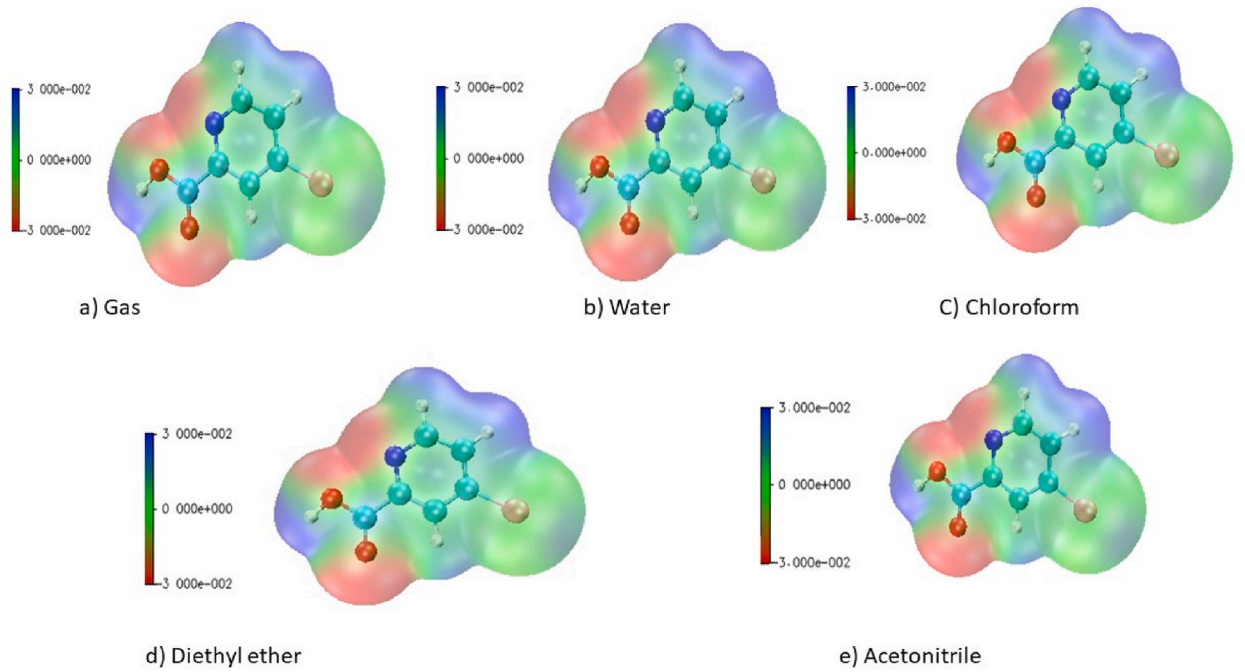

Fig. 2. ESP map of 5BNA in the a) gas phase and with different solvents media b) Water c) Chloroform d) Diethyl ether and e) Acetonitrile.

Table 1
Mulliken atomic charges, Fukui functions and local softness of 5BNA.

Atoms	Mulliken atomic charges			Fukui functions				Local softness		
	0, 1 (N)	N +1 (−1, 2)	N-1 (1,2)	f_p^+	f_p^-	f_p^0	Δf	$s_p + f_p^+$	s_p- f_p^--	s_p^0 f_p^0
Br1	0.1173	−0.0292	0.2495	−0.1465	−0.1322	−0.1393	−0.0142	−0.0306	−0.0276	−0.0291
O2	−0.4147	−0.4653	−0.3656	−0.0506	−0.0491	−0.0498	−0.0016	−0.0106	−0.0103	−0.0104
O3	−0.4779	−0.6189	−0.2927	−0.1410	−0.1851	−0.1631	0.0441	−0.0295	−0.0387	−0.0341
N4	−0.1122	−0.2149	0.1216	−0.1027	−0.2338	−0.1682	0.1311	−0.0215	−0.0489	−0.0352
C5	−0.6421	−0.8572	−0.5662	−0.2151	−0.0760	−0.1455	−0.1392	−0.0450	−0.0159	−0.0304
C6	0.8699	0.8845	0.9428	0.0145	−0.0729	−0.0292	0.0874	0.0030	−0.0152	−0.0061
C7	−0.4815	−0.5463	−0.3655	−0.0648	−0.1159	−0.0904	0.0511	−0.0136	−0.0242	−0.0189
C8	−0.2739	−0.4850	−0.2542	−0.2110	−0.0198	−0.1154	−0.1913	−0.0441	−0.0041	−0.0241
C9	0.0578	0.0827	0.0628	0.0250	−0.0051	0.0099	0.0301	0.0052	−0.0011	0.0021
C10	0.4284	0.5112	0.3388	0.0829	0.0896	0.0862	−0.0067	0.0173	0.0187	0.0180
H11	0.2197	0.1828	0.2515	−0.0369	−0.0319	−0.0344	−0.0050	−0.0077	−0.0067	−0.0072
H12	0.1454	0.0927	0.2002	−0.0527	−0.0548	−0.0538	0.0021	−0.0110	−0.0115	−0.0112
H13	0.1627	0.1037	0.2372	−0.0590	−0.0745	−0.0667	0.0156	−0.0123	−0.0156	−0.0140
H14	0.4012	0.3592	0.4398	−0.0421	−0.0386	−0.0403	−0.0035	−0.0088	−0.0081	−0.0084

between O3–H14 is an intermolecular interaction, especially a partial link such as a hydrogen bond. In Br1–C7, the longer bond length with the carbon atom results from the presence of bromine, which is heavy in size and has a decreased electronegativity. The presence of the Br atom in NA increases the chemical stability of the nicotinic acid. Because of the lower attraction between the electrons in both atoms, bond length increases causing less stability. The shortest bond length is observed for the hydrogens bound to aromatic carbons (C6–H11, C8–H12 and C9–H13) and the oxygen atom of the carboxylic acid group (O2–H14). These hydrogens bound to aromatic carbons are non-polar and form the fundamental linkage of the compound's structure by making it stable. The O–H bond is more polar and more effective because its electronegativity differences are bigger. The strength and stability of an atomic bond increase as the length of that bond decrease because the electrons are closer to the nucleus and thus leading to a stronger bond between the atoms. The theoretically measured important bond angles (highest) are at C4–C9–C8, O2–C10–O3, C7–C6–H11 and C7–C8–H12 signifies more stability.

3.2. Reactivity analysis

The electrostatic potential is characterized as the interaction vitality between the charge dissemination of a molecule and a unit positive charge. It gives important details concerning the atomic and electronic charge dispersion of a given atom and is used as a

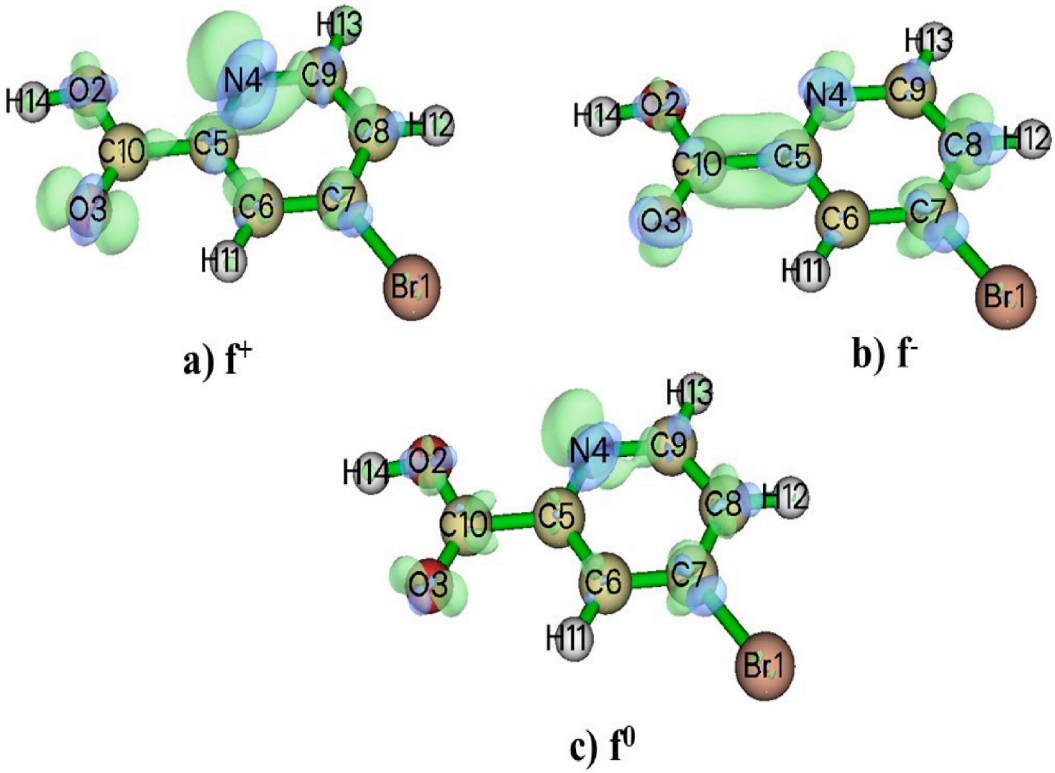

Fig. 3. Fukui functions f^{+}, f^{-} and f^{0} of 5BNA.

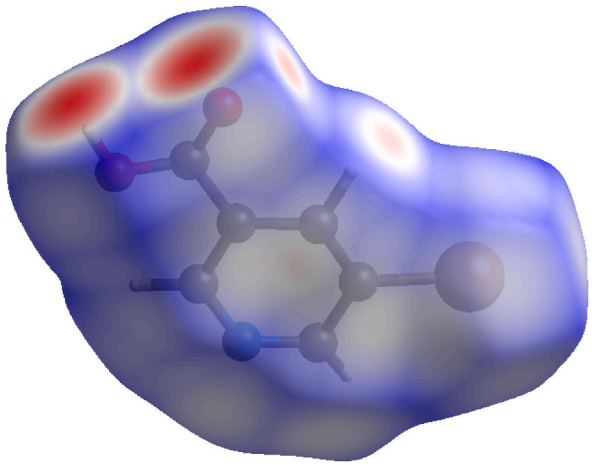

Fig. 4. Hirshfeld surface of 5BNA.

technique for interpreting and predicting the type of chemical reactivity [23]. It is utilised to determine the origin of chemical bonding and intermolecular interactions [24]. ESP map consists of the colour grading representation for defining the charge distribution of the molecule. The blue indicates the high concentration of electrons (nucleophile), red as a low high concentration of electrons (electrophile) and green serves as an intermedial stage (neutral region). According to Fig. 2 [25], the electron deficit site is found at the oxygen atoms of the carboxylic acid region and the nitrogen atom of the molecule in both gas and other solvents. The electron donor site with positive potential is majorly found at hydrogen atoms bound to aromatic carbon present in the molecule.

The Fukui function gives details on the reactivity zones contained within the molecule as well as a model for evaluating chemical reaction mechanisms. Atoms that donate electrons (nucleophiles) and accept electrons (electrophiles) are easily distinguished [26]. Under Mulliken charge analysis, each atom will be allocated a number. Simplified Fukui functions are used for radical-f_p^0,

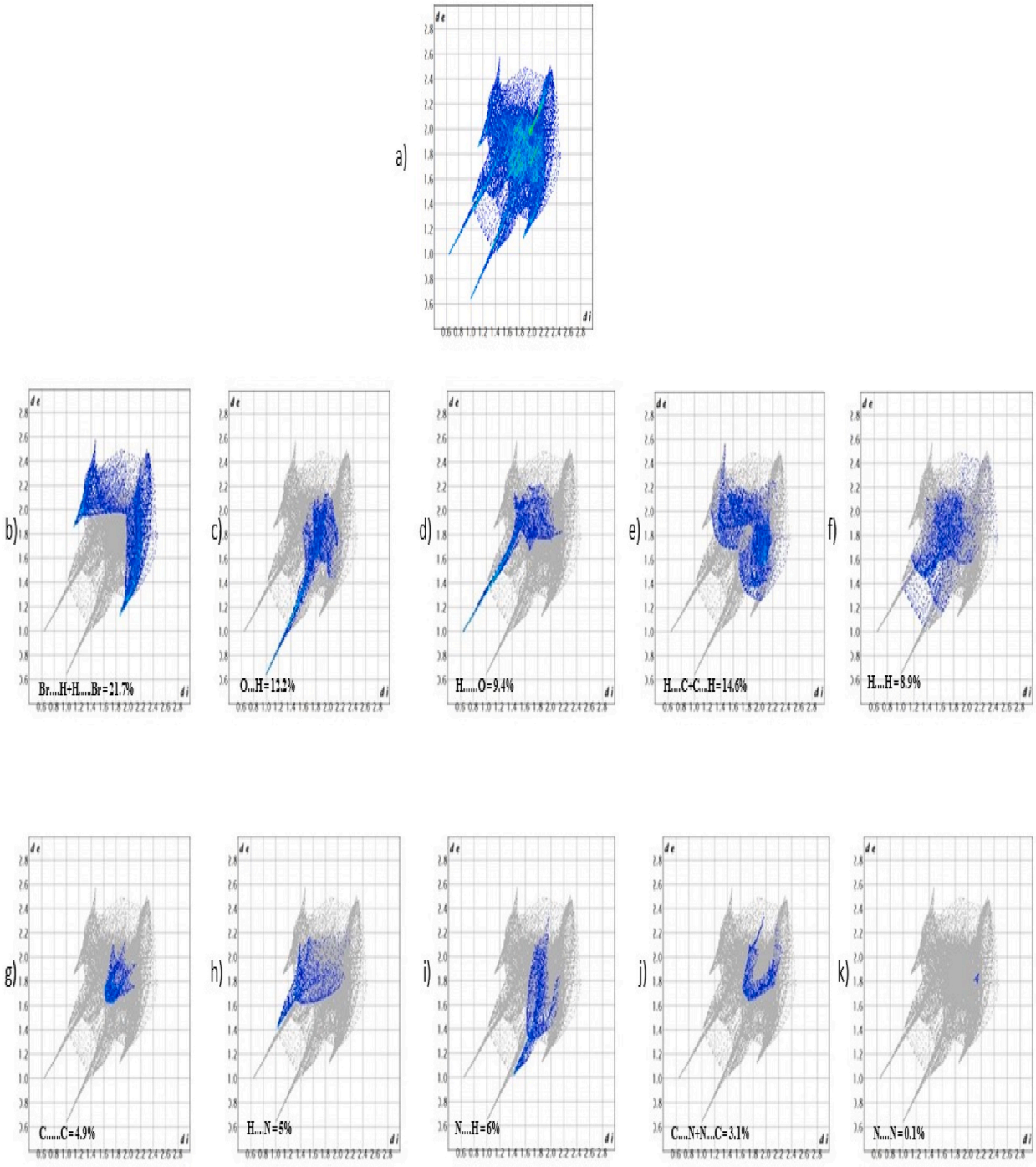

Fig. 5. 2D fingerprint plots indicating the intermolecular interactions of a) 5BNA molecule, b) Br···H + H···Br, c) O···H, d) H···O, e) H···C + C···H, f) H···H g) C···C h) H···N i) N···H j) C···N + N···C and k) N···N.

electrophile-f_p^- and nucleophile – f_p^+ attacks on the pth atom site[27,27,27].

$$f_p^+ = q_p\,(N) - q_p\,(N-1) \tag{1}$$

$$f_p^- = q_p\,(N+1) - q_p\,(N) \tag{2}$$

Table 2
2D Fingerprint percentage of 5BNA.

Inside Atom↓/Outside Atom →	Br	C	N	O	H
Br	6.10%	1.20%	–	–	13.80%
C	1.10%	4.10%	1.70%	1.80%	8.70%
N	–	1.30%	0.10%	–	6%
O	–	1.40%	–	3.30%	12.20%
H	7.80%	5.90%	5%	9.40%	8.90%

Table 3
NLO parameters of 5BNA in the gas phase and with various solvent media.

Parameters	Gas	Water	Chloroform	Diethyl ether	Acetonitrile
μ_x (D)	0.35186	0.55790	0.48396	0.47762	0.55102
μ_y (D)	0.58966	0.77062	0.72566	0.71964	0.76717
μ_z (D)	0.00002	0.00005	0.00006	0.00009	0.00845
μ (D)	0.68666	0.95138	0.87224	0.86371	0.94459
α_{xx} (esu)	21.00139	27.71384	25.67112	25.46423	27.53491
α_{yy} (esu)	−0.23235	−0.73495	−0.54473	−0.52806	−0.71670
α_{zz} (esu)	16.33624	22.64990	20.53358	20.32941	22.45711
$< \alpha >$ (esu)	12.36843	16.54293	15.21999	15.08853	16.42511
Δα (esu)	184.44068	250.82966	229.61418	227.52652	248.92869
β_{xxx} (esu)	−1852.94378	−5218.00726	−3934.46555	−3816.96459	−5094.45703
β_{xyy} (esu)	−287.30040	−18.55544	−221.38512	−232.02122	−43.28859
β_{xzz} (esu)	−293.29485	−1283.86292	−888.60532	−855.19786	−1244.91253
β_{yyy} (esu)	236.63566	−78.41278	109.17092	122.43964	−57.13575
β_{xxy} (esu)	−0.40123	−0.18627	0.45900	0.08447	−0.11579
β_{yzz} (esu)	−0.14443	0.47921	0.41877	0.59008	0.48225
β_{zzz} (esu)	0.48923	0.83266	0.66962	0.71868	1.01910
β_{xxz} (esu)	383.39921	511.57873	478.62209	475.39653	509.36046
β_{yyz} (esu)	135.86564	233.14323	189.18730	185.83825	228.49034
$< \beta >$ (esu)	2499.59898	6563.37602	5089.74568	4950.18757	6425.53316

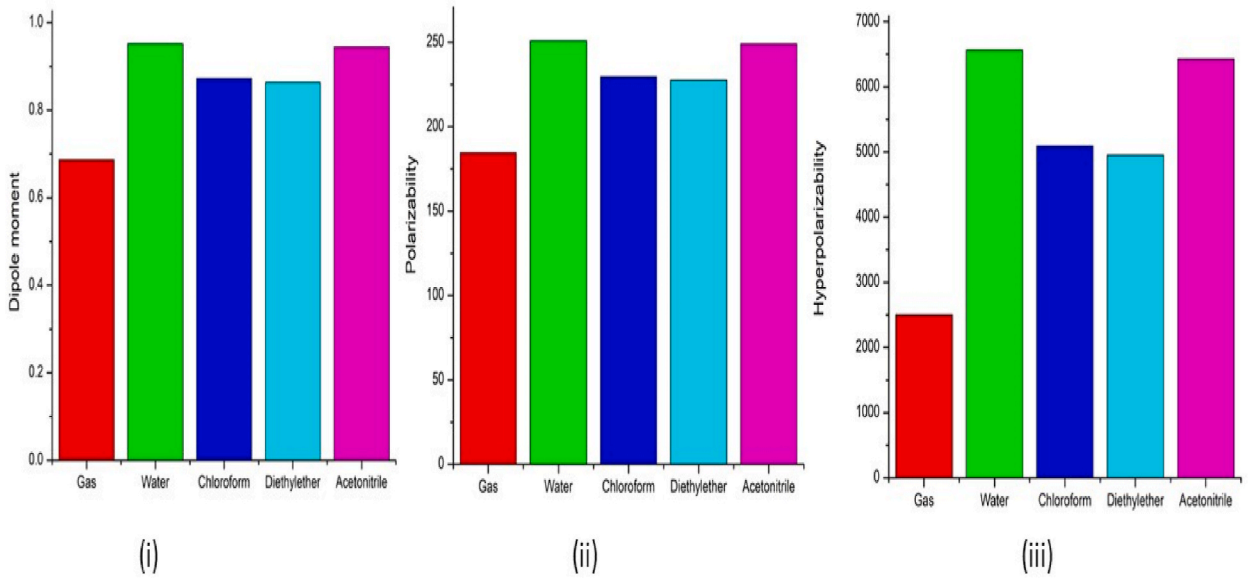

Fig. 6. (i) Dipole moment, (ii) Polarizability and (iii) Hyperpolarizability of 5BNA in the gas phase and with different solvents media.

$$f_p^0 = \frac{1}{2}\left(q_p\,(N+1) - q_p\,(N-1)\right) \tag{3}$$

The dual descriptor, which is calculated as $\Delta f = f_p^{+} - f_p^{-}$, can accurately distinguish between nucleophilic and electrophilic locations present in the molecule. The negative values ($\Delta f < 0$) of 5BNA (gas Phase) are electrophile, whereas the positive values ($\Delta f > 0$) are nucleophile, as shown in Table 1. In accordance with Fig. 3 [28], the blue portions represent negative regions that are vulnerable to

Table 4
Second-order perturbation theory analysis of Fock matrix in NBO basis of 5BNA in the gas phase.

Donar (i)	Type	ED/e	Acceptor (j)	Type	ED/e	E(2) (Kcal/mol)	E(*j*)-E(i) (a.u)	F(i,j) (a.u)
Br1 – C7	σ	1.98517	C5 – C6	σ*	0.03307	2.6	1.21	0.05
Br1 – C7	σ	1.98517	C8 – C9	σ*	0.02823	2.56	1.21	0.05
O2–C10	σ	1.99535	O3–C10	σ*	0.01871	0.6	1.55	0.027
O2–C10	σ	1.99535	C5 – C6	σ*	0.03307	1.25	1.49	0.039
O2–H14	σ	1.98565	O3–C10	σ*	0.01871	1.05	1.36	0.034
O2–H14	σ	1.98565	C5–C10	σ*	0.07929	4.03	1.14	0.061
O3–C10	σ	1.9959	N4–C5	σ*	0.02199	1.11	1.61	0.038
O3–C10	σ	1.9959	C5–C10	σ*	0.07929	1.51	1.48	0.043
O3–C10	π	1.9959	O3–C10	π*	0.23911	0.76	0.4	0.016
O3–C10	π	1.9959	C5 – C6	π*	0.32453	3.22	0.4	0.035
N4–C5	σ	1.98467	O3–C10	σ*	0.01871	1.12	1.45	0.036
N4–C5	σ	1.98467	N4–C9	σ*	0.01434	1.01	1.38	0.033
N4–C5	σ	1.98467	C5 – C6	σ*	0.03307	2.75	1.39	0.055
N4–C5	σ	1.98467	C5–C10	σ*	0.07929	0.56	1.23	0.024
N4–C5	σ	1.98467	C6–H11	σ*	0.01416	1.29	1.28	0.036
N4–C5	σ	1.98467	C9–H13	σ*	0.02358	2.11	1.26	0.046
N4–C9	σ	1.98621	N4–C5	σ*	0.02199	1.15	1.37	0.035
N4–C9	σ	1.98621	C5–C10	σ*	0.07929	3.08	1.23	0.056
N4–C9	σ	1.98621	C8 – C9	σ*	0.02823	1.53	1.39	0.041
N4–C9	σ	1.98621	C8–H12	σ*	0.01349	1.34	1.26	0.037
N4–C9	π	1.98621	C5 – C6	π*	0.32453	26.25	0.32	0.082
N4–C9	π	1.98621	C7–C8	π*	0.36456	14.6	0.31	0.061
C5 – C6	σ	1.96919	Br1 – C7	σ*	0.03807	6.08	0.8	0.063
C5 – C6	σ	1.96919	O2–C10	σ*	0.08968	1.49	1.08	0.036
C5 – C6	σ	1.96919	N4–C5	σ*	0.02199	2.58	1.25	0.051
C5 – C6	σ	1.96919	C5–C10	σ*	0.07929	1.2	1.11	0.033
C5 – C6	σ	1.96919	C6–C7	σ*	0.02557	3.42	1.27	0.059
C5 – C6	σ	1.96919	C6–H11	σ*	0.01416	1.2	1.16	0.033
C5 – C6	π	1.96919	O3–C10	π*	0.23911	16.57	0.28	0.063
C5 – C6	π	1.96919	N4–C9	π*	0.3576	18.51	0.27	0.064
C5 – C6	π	1.96919	C7–C8	π*	0.36456	22.07	0.27	0.069
C5–C10	σ	1.97386	O2–H14	σ*	0.01002	2.06	1.06	0.042
C5–C10	σ	1.97386	O3–C10	σ*	0.01871	1.17	1.28	0.035
C5–C10	σ	1.97386	N4–C5	σ*	0.02199	1.12	1.19	0.033
C5–C10	σ	1.97386	N4–C9	σ*	0.01434	3.28	1.2	0.056
C5–C10	σ	1.97386	C5–C6	σ*	0.03307	1.02	1.21	0.031
C5–C10	σ	1.97386	C6–C7	σ*	0.02557	2.41	1.22	0.048
C6–C7	σ	1.97989	C5–C6	σ*	0.03307	2.91	1.29	0.055
C6–C7	σ	1.97989	C5–C10	σ*	0.07929	2.17	1.14	0.045
C6–C7	σ	1.97989	C6–H11	σ*	0.01416	1.64	1.19	0.039
C6–C7	σ	1.97989	C7–C8	σ*	0.02656	3.09	1.3	0.057
C6–C7	σ	1.97989	C8–H12	σ*	0.01349	2.41	1.17	0.048
C6–H11	σ	1.97521	N4–C5	σ*	0.02199	5.07	1.06	0.065
C6–H11	σ	1.97521	C5–C6	σ*	0.03307	0.95	1.08	0.029
C6–H11	σ	1.97521	C6–C7	σ*	0.02557	1.44	1.09	0.035
C6–H11	σ	1.97521	C7–C8	σ*	0.02656	4.09	1.09	0.059
C7–C8	σ	1.98103	C6–C7	σ*	0.02557	3.07	1.3	0.057
C7–C8	σ	1.98103	C6–H11	σ*	0.01416	2.48	1.19	0.049
C7–C8	σ	1.98103	C8–C9	σ*	0.02823	2.46	1.3	0.051
C7–C8	σ	1.98103	C8–H12	σ*	0.01349	1.48	1.17	0.037
C7–C8	σ	1.98103	C9–H13	σ*	0.02358	1.8	1.17	0.041
C7–C8	π	1.65299	N4–C9	π*	0.3576	23.92	0.29	0.074
C7–C8	π	1.65299	C5–C6	π*	0.32453	18.97	0.3	0.068
C8–C9	σ	1.97493	Br1 – C7	σ*	0.03807	6.09	0.81	0.063
C8–C9	σ	1.97493	N4–C9	σ*	0.01434	1.38	1.26	0.037
C8–C9	σ	1.97493	C7–C8	σ*	0.02656	3.4	1.27	0.059
C8–C9	σ	1.97493	C8–H12	σ*	0.01349	0.97	1.15	0.03
C8–C9	σ	1.97493	C9–H13	σ*	0.02358	0.83	1.14	0.027
C8–H12	σ	1.9783	N4–C9	σ*	0.01434	4.12	1.08	0.06
C8–H12	σ	1.9783	C6–C7	σ*	0.02557	4.09	1.09	0.06
C8–H12	σ	1.9783	C7–C8	σ*	0.02656	1.21	1.09	0.032
C8–H12	σ	1.9783	C8–C9	σ*	0.02823	0.69	1.09	0.025
C9–H13	σ	1.98082	N4–C5	σ*	0.02199	4.75	1.06	0.063
C9–H13	σ	1.98082	C7–C8	σ*	0.02656	3.37	1.08	0.054
Br1	LP(1)	1.99325	C6–C7	σ*	0.02557	1.62	1.55	0.045
Br1	LP(1)	1.99325	C7–C8	σ*	0.02656	1.72	1.55	0.046
Br1	LP(2)	1.97477	C7–C8	σ*	0.02656	3.49	0.85	0.049

(*continued on next page*)

Table 4 (*continued*)

Donar (i)	Type	ED/e	Acceptor (j)	Type	ED/e	E(2) (Kcal/mol)	E(*j*)-E(i) (a.u)	F(i,j) (a.u)
Br1	LP(2)	1.97477	C7–C8	σ*	0.02656	3.44	0.85	0.048
Br1	LP(3)	1.92328	C7–C8	π*	0.36456	10.96	0.3	0.055
O2	LP(1)	1.97671	O3–C10	σ*	0.01871	6.91	1.23	0.082
O2	LP(2)	1.8096	O3–C10	π*	0.23911	47.29	0.34	0.115
O3	LP(1)	1.98034	O2–C10	σ*	0.08968	1.32	1.06	0.034
O3	LP(1)	1.98034	C5–C10	σ*	0.07929	2.09	1.1	0.043
O3	LP(2)	1.85334	O2–C10	σ*	0.08968	31.71	0.63	0.128
O3	LP(2)	1.85334	C5–C10	σ*	0.07929	18.29	0.66	0.1
N4	LP(1)	1.9125	C5–C6	σ*	0.03307	10.23	0.89	0.086
N4	LP(1)	1.9125	C5–C10	σ*	0.07929	3.8	0.74	0.047
N4	LP(1)	1.9125	C8–C9	σ*	0.02823	9.3	0.89	0.083
N4	LP(1)	1.9125	C9–H13	σ*	0.02358	4.22	0.77	0.052

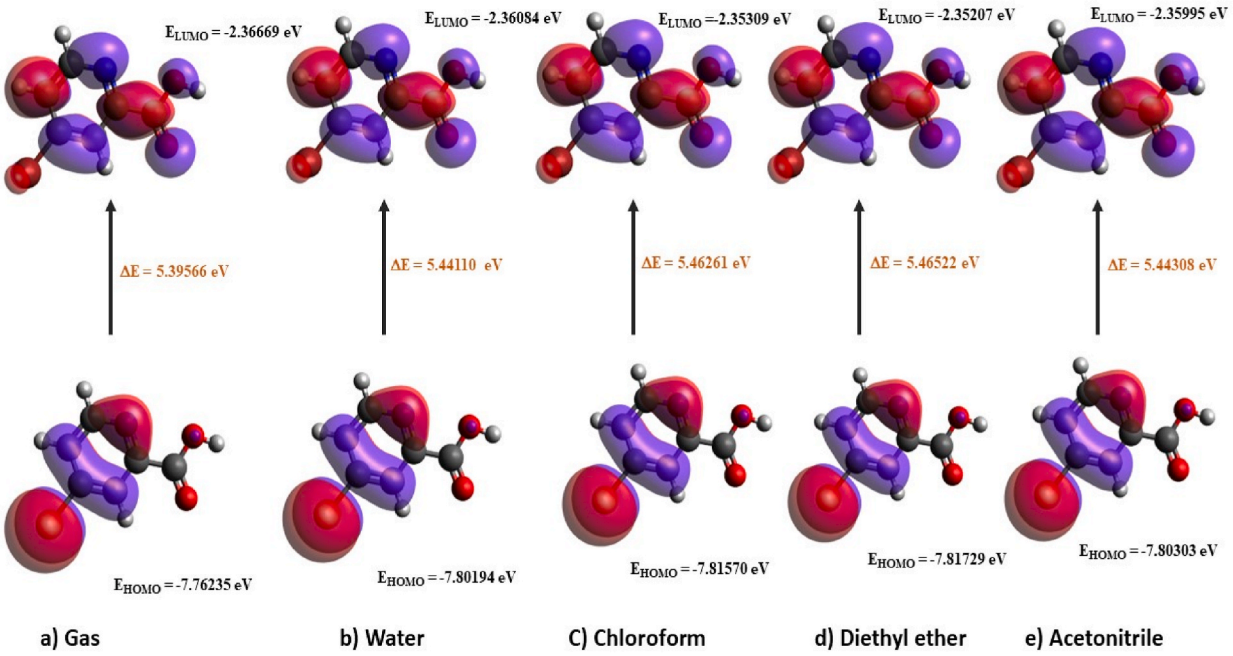

Fig. 7. HOMO and LUMO plot 5BNA in the a) gas phase and with different solvents media b) Water c) Chloroform d) Diethyl ether and e) Acetonitrile.

Table 5
Calculated energy values of 5BNA in the gas phase and with various solvent media.

Parameters	Gas	Water	Chloroform	Diethyl ether	Acetonitrile
HOMO (eV)	−7.76235	−7.80194	−7.81570	−7.81729	−7.80303
LUMO (eV)	−2.36669	−2.36084	−2.35309	−2.35207	−2.35995
Ionisation potential (eV)	7.76235	7.80194	7.81570	7.81729	7.80303
Electron affinity (eV)	2.36669	2.36084	2.35309	2.35207	2.35995
Energy gap (eV)	5.39566	5.44110	5.46261	5.46522	5.44308
Electronegativity (eV)	5.06452	5.08139	5.08439	5.08468	5.08149
Chemical potential (eV)	−5.06452	−5.08139	−5.08439	−5.08468	−5.08149
Chemical hardness (eV)	2.69783	2.72055	2.73131	2.73261	2.72154
Chemical softness (eV)	0.18533	0.18379	0.18306	0.18298	0.18372
Electrophilicity index (eV)	4.75370	4.74546	4.73236	4.73064	4.74392
Electronic charge (eV)	−1.87726	−1.86778	−1.86152	−1.86074	−1.86714
Electron donating capability (w +) (eV)	7.62319	7.62622	7.61597	7.61455	7.62485
Electron accepting capability (w-) (eV)	2.55867	2.54483	2.53158	2.52987	2.54336

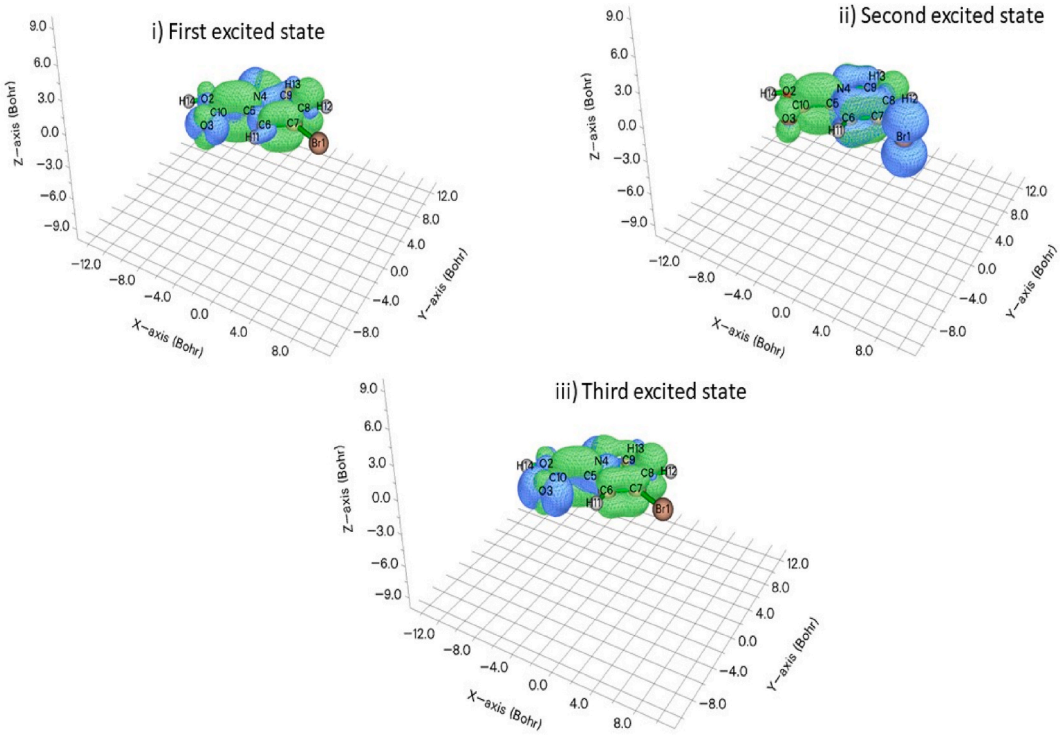

Fig. 8. Charge distribution for (i) first, (ii) second and (iii) third excited states for 5BNA in the gas phase.

Table 6
Excitation energy (E), D index, Δr index, t index for different excited states for 5BNA gas phase.

Parameters	First excited state	Second excited state	Third excited state
Excitation energy - E (eV)	4.144	4.799	4.833
Charge transfer length- D index (Å)	0.839	1.963	1.539
Δr index (Å)	0.839	2.079	1.318
τ index (Å)	−0.595	0.292	0.099
H index (Å)	2.130	2.237	2.187
S_m index (a.u)	0.25617	0.44417	0.22969
S_r index (a.u)	0.51805	0.67993	0.48146

attacks caused by electrophiles and the green portions represent positive regions that are vulnerable to attacks caused by nucleophiles. In 5BNA, electrophiles are located at Br1, O2, C5, C8, H11 and H14 and the nucleophiles are located at O3, N4, C6, C7, C9, H12 and H13. The local softness of the compound is directly associated with the Fukui function of the compound and the maximum local softness is found at C10 = 0.018737.

3.3. Hirshfeld surface analysis

Hirshfeld surface is an effective method for investigating the interactions in the molecular crystal as the surface is characterized by both the confined molecule and its closest neighbouring atoms [29]. The 3D structural information of 5BNA is provided by various properties such as d_e (0.6434–2.6094), d_i (0.6419–2.4828), curvedness (−4.0322–0.3046), shape index (−0.9968–0.9982), fragment's colour patch (0.0000–13.0000) (Fig. S1) and d_{norm} (−0.7504–0.9593). The red patches in Fig. 4 [30] reflect the region with the most interactions between hydrogen bonds because they represent the closer link among the closest nearby atoms. The red patch encompassing the C═O and O–H bonds indicates how tight the bonds are and how much stronger the intermolecular interactions will be as a result of their presence. The white region depicts the Vander Walls partition, whereas the blue region indicates the molecule's wider interconnectedness [31]. The percentage of each type of intermolecular interaction on the molecule's surface is displayed in the 2D fingerprint plots in Fig. 5 [32] and Table 2. Br ….H and H …..Br together constitutes 21.7% of the primary fingerprint region. The major lowest peak was provided by a 12.2% contribution from O···H and the highest peak was provided by a 9.4% contribution from H …..O. In the middle, the H ….C and C ….H comprise 14.6%. H ….H interactions contribute 8.9% and C …..C interactions contribute 4.9%. H ….N contributes 5% and N ….H contributes 6% to a significant peak in the centre. C ….N and N ….C provide 3.1% collectively, with N ….N contributing the least at 0.1%.

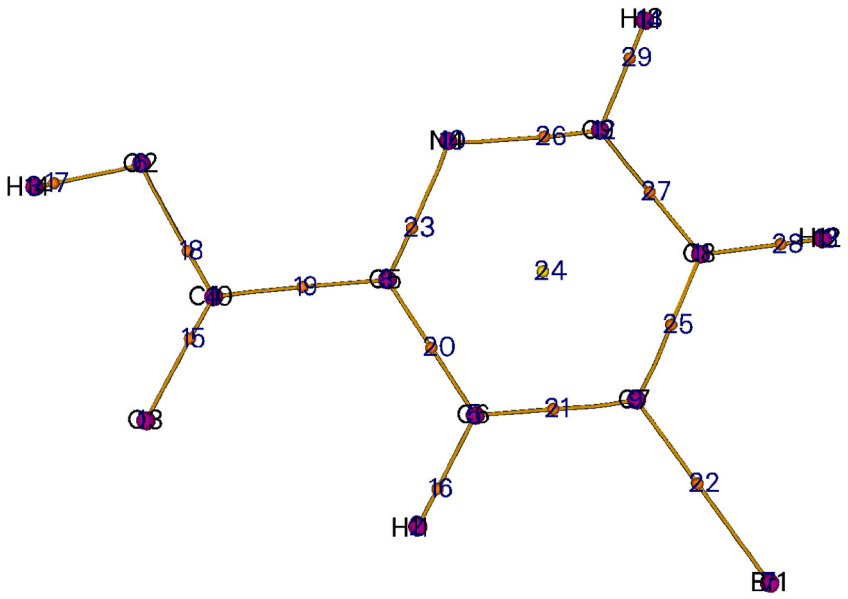

Fig. 9. AIM of 5BNA in the gas phase.

3.4. Non-linear optics

Non-linear optics is the evaluation of phenomena that develop as a result of light's influence altering a material's optical characteristics. It focuses on the theoretical underpinnings regulating the tensor properties of a molecule's polarisation capability [33,34]. Table 3 demonstrates the calculated NLO parameters such as dipole moment (μ), polarizability (α) and hyperpolarizability (β) of 5BNA with the various solvents. The calculated values of μ,α and β of 5BNA in the gas phase are 0.68666D, 16.54292 × 10^{-24} esu and 2499.598978 × 10^{-33} esu. With the addition of solvents like water (0.95138D, 250.82966 × 10^{-24} esu and 6563.37602 × 10^{-33} esu), chloroform (0.87223D, 229.61418 × 10^{-24} esu and 6563.37602 × 10^{-33} esu), diethyl ether (0.86371D, 227.5265 × 10^{-24} esu and 4950.187567 × 10^{-33} esu) and acetonitrile (0.944589D, 248.92869 × 10^{-24} esu and 6425.53316 × 10^{-33} esu), the μ,α and β show a rise by transitioning from the gas to the solution phases (Fig. 6) [35]. 5BNA with various solvents could serve as a suitable NLO compound and its large α, β and no null values of μ suggest that it belongs to an essential group of compounds in pharmaceutical science. Moreover, in comparison with nicotinic acid, 5BNA shows high enhancement as the bromine atom in the 5BNA acts as an electron-withdrawing group [36]. The prediction of μ plays a significant subject related to the stability of the molecule [37]. These obtained findings are made to compare with the urea as the model and it is noticed that the 5BNA in gas and with solvents have larger values of α and β [38]. As a result, it is possible 5BNA will be useful for research on optical properties that are nonlinear over the forthcoming years.

3.5. NBO

NBO investigations are an effective technique for examining inter and intramolecular linkages, as they offer a valuable foundation for investigating the transfer of charge in molecules [39]. It provides a strong analytical approach that produces a comprehensible chemical depiction of complicated electronic structures in an instinctual way. The charge transfer between the accepting proton and anti-bonding orbitals of the donating proton is emphasised in NBO analysis [40]. The following equation is used in NBO analysis to calculate the E(2) (stabilisation energy) is[41].

$$\Delta E_{ij} = E(2) = q_i \frac{F_{ij}^2}{E_j - E_i}$$

E_j and E_i represent the energies of acceptor and donor energies, F_{ij} is the Fock matrix's diagonal elements and q_i is the occupancy of donor Lewis's type orbital. Higher E(2) values indicate more effective, greater interactions of donor and acceptor [42]. From Table 4, the following that contributes most to molecule stability comprise LP (lone pair) O2→ π* O3–C10 with 47.29 kcal/mol, LP O3→ π* O2–C10 with 31.71 kcal/mol, π N4–C9→ π* C5–C6 with 26.25 kcal/mol, π C7–C8→ π* N4–C9 with 23.92 kcal/mol, π C5 – C6→ π* C7–C8 with 22.07 kcal/mol, π C5–C6→ π* N4–C9 with 18.51 kcal/mol, LP O3→ σ* C5–C10 with 18.29 kcal/mol, π C5 – C6→ π* O3–C10 with 16.57 kcal/mol and from π N4–C9→ π* C7–C8 with 14.6 kcal/mol. The other interactions, σ C8–C9→ σ* Br1 – C7 with 6.09 kcal/mol, σ C5 – C6→ σ* Br1 – C7 with 6.08 kcal/mol, σ C6–H11→ σ* N4–C5 with 5.07 kcal/mol and from σ C9–H13→ σ* N4–C5 with 4.75 kcal/mol. The interactions coming from lone pairs of electrons on heteroatoms to π* orbitals are those that are vital and have the highest degree of stability. Within this molecule, further stabilising charge transfers are shown to take place at the C7–C8's π and π*

Table 7
Electron density and Laplacian electron density of 5BNA in the gas phase and with various solvent media.

Atom	Gas		Water		Chloroform		Diethyl ether		Acetonitrile	
	ρ (a. u)	$\nabla^2\rho$(a. u)	ρ (a. u)	$\nabla^2\rho$(a. u)	ρ (a. u)	$\nabla^2\rho$(a. u)	ρ (a. u)	$\nabla^2\rho$(a. u)	ρ (a. u)	$\nabla^2\rho$(a. u)
O2–H14	0.359031	−0.251688	0.355313	−0.252854	0.3564142	−0.252553	0.356576	−0.252567	0.355362	−0.251448
O2–C10	0.305729	−0.501934	0.307438	−0.493079	0.3070659	−0.495757	0.307029	−0.49629	0.30741	−0.49333
O3–C10	0.41636	−0.214213	0.412777	−0.228969	0.4137293	−0.225175	0.413931	−0.223803	0.412854	−0.228674
C10–C5	0.26296	−0.664852	0.263622	−0.668103	0.263442	−0.66727	0.263339	−0.666716	0.263609	−0.668046
C5–N4	0.34326	−0.100652	0.341513	−0.100053	0.3422455	−0.100292	0.342306	−0.100316	0.341586	−0.100076
N4–C9	0.342635	−0.964449	0.340472	−0.94527	0.3411278	−0.951498	0.341372	−0.95201	0.340532	−0.94583
C9–H13	0.286065	−0.10036	0.287448	−0.101483	0.2870566	−0.101162	0.286949	−0.101082	0.287415	−0.101456
C8–C9	0.309073	−0.860643	0.309311	−0.863865	0.3092728	−0.863062	0.309204	−0.862616	0.309308	−0.8638
C8–H12	0.28383	−0.98703	0.285118	−0.999301	0.2847054	−0.995335	0.284643	−0.994801	0.285081	−0.998947
C7–C8	0.311499	−0.875077	0.312319	−0.880588	0.3120177	−0.878589	0.311988	−0.878358	0.312291	−0.880405
Br1–C7	0.158302	−0.144144	0.158176	−0.144742	0.1581832	−0.144537	0.158217	−0.144579	0.158176	−0.144724
C6–C7	0.312347	−0.87909	0.312204	−0.879083	0.3122671	−0.879141	0.312201	−0.878724	0.312209	−0.879079
C6–H11	0.286087	−0.100566	0.286499	−0.100891	0.2863803	−0.100802	0.286355	−0.100784	0.286488	−0.100883
C5–C6	0.308386	−0.853055	0.309105	−0.856847	0.3088201	−0.855328	0.308823	−0.85533	0.309079	−0.856704

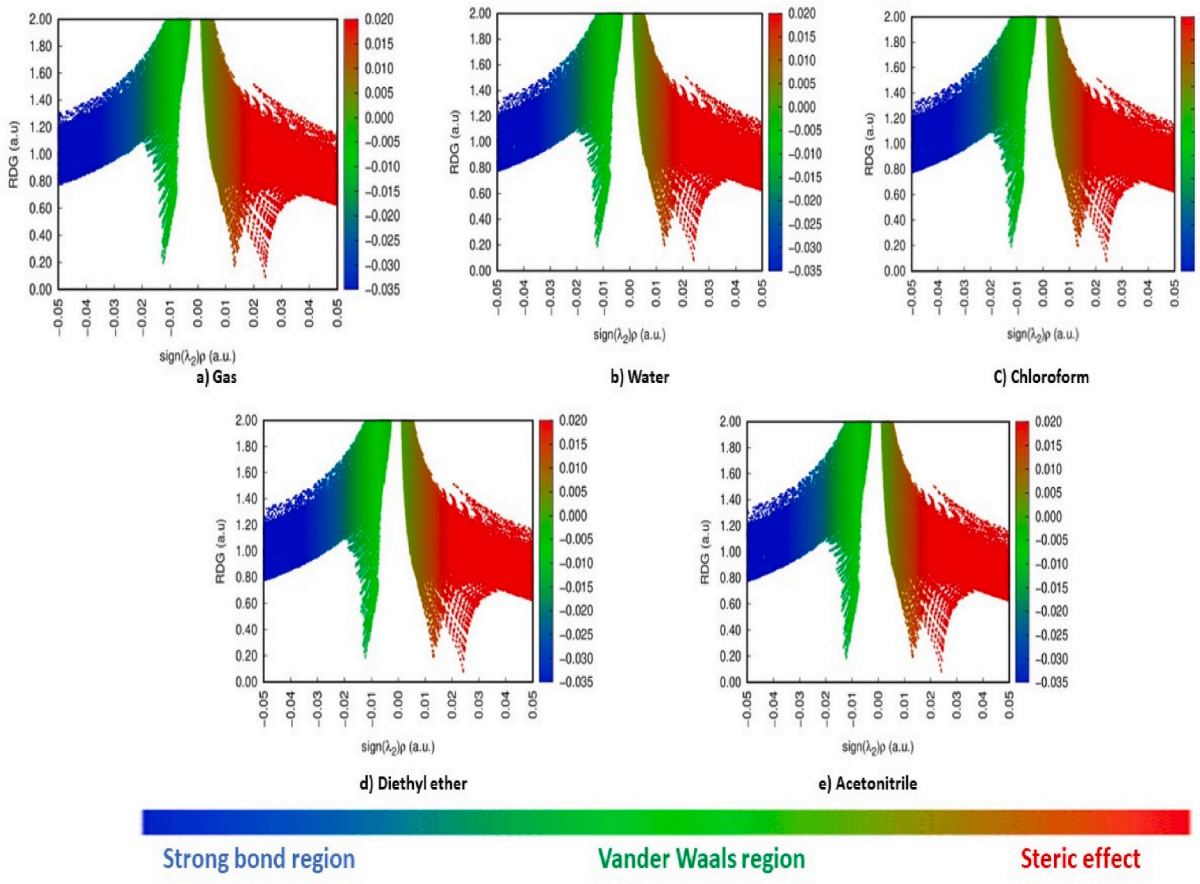

Fig. 10. RDG map of 5BNA in the a) gas phase and with different solvents media b) Water c) Chloroform d) Diethyl ether and e) Acetonitrile.

orbitals in particular, with the majority of these being π and π* transitions.

3.6. MO studies

MO (Molecular orbital) is extremely important in the determination of the optical, chemical and electrical characteristics of a molecule and also performs a crucial role in chemical processes [43]. This can also be utilised to project the highest reacting point in a system of π electrons and explicate many forms of conjugate reactions. The HOMO symbolises donating electrons, whereas LUMO draws in electrons in interactions with the molecule [44]. The obtained energy difference (Fig. 7) [45] values are 5.39566 eV (gas), 5.44110 eV (water), 5.46261 eV (chloroform), 5.46522 eV (diethyl ether) and 5.44308 eV (acetonitrile). The electron affinity is indicated by HOMO and the ionisation potential is indicated by the LUMO. From Table 5, the ionisation potential shows a very minor change in the gas and solvent phase of 5BNA and it is greater compared to the electron affinity, showing that it could behave as a nucleophile. The molecule's stability can be inferred from its elevated chemical hardness and lower chemical softness values. The diethyl ether acquires a high energy difference of 5.46522 eV compared with other solvents. The band gap increases as the order of polarity of solvent rises, i.e., gas phase < water < acetonitrile < chloroform < diethyl ether. Moreover, the most significant increase in chemical hardness and decrease in the chemical softness of the 5BNA occurs in diethyl ether, making it stronger and less susceptible to adverse effects owing to increased chemical activity.

3.7. Charge transfer analysis

The inspection of the electron-hole distributions and their visual representation in all three excited states within the molecule is performed using Multiwfn 3.7 application to investigate charge transfer caused by excitation inside the molecule. Fig. 8 [46] and Table 6 depict the electron-hole distributions of 5BNA. The value of the D index for S1 is 0.839 Å, which is nearly half of the value of the C–C bond of 5BNA. Whereas, the D index values of S2 and S3 are greater than 1 and it represents the transfer of charges in the molecule. The H-index measures the width of the mean hole and electron dispersion. All three states S1, S2 and S3 show the excitations are clearly broader, and hence the H index values are higher. The S_r index exceeds 0.5 (<1) during the first two excited states, indicating that

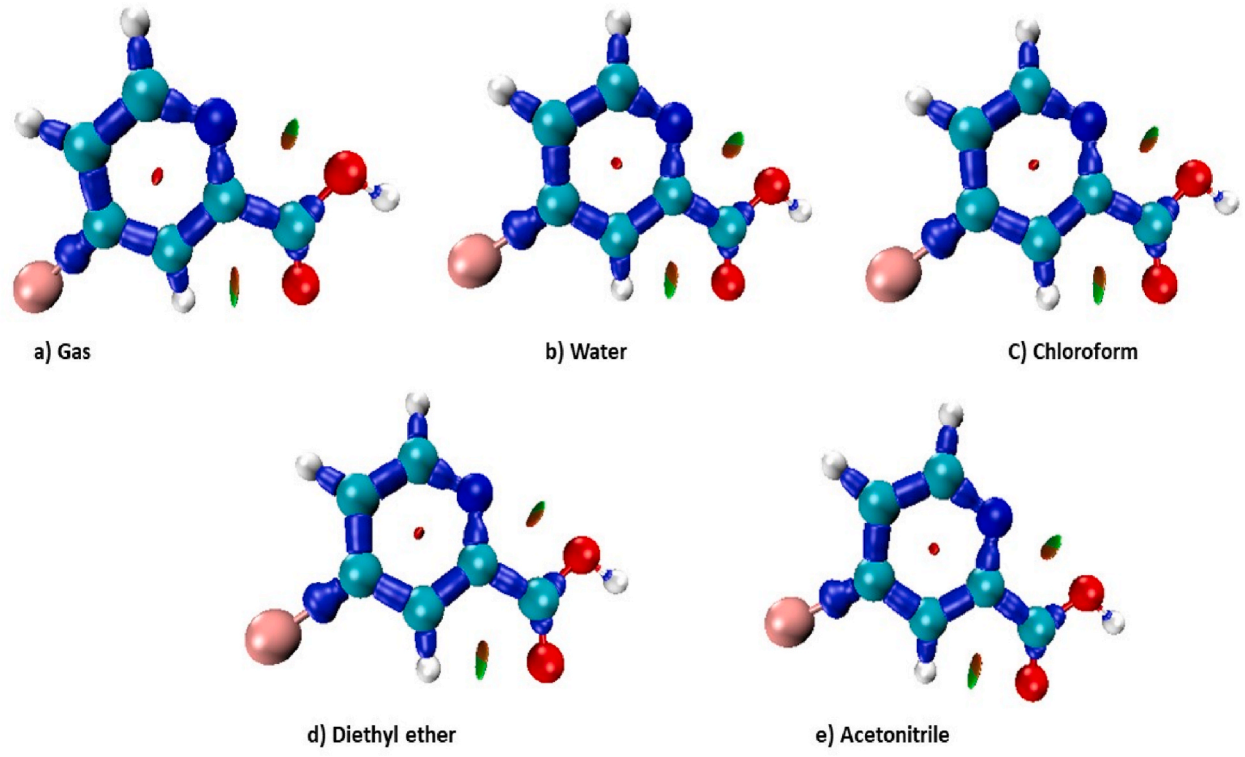

Fig. 11. IRI isosurface of 5BNA in the a) gas phase and with different solvents media b) Water c) Chloroform d) Diethyl ether and e) Acetonitrile.

nearly half of a hole and electron have the correct match. The positive values of the τ index indicate the hole and electron separation with the charge transfer. D index demonstrates the length of the charge transfer. A large D index value signifies the length of the hole and electron is greater. and it is observed for S2. The centroid distance between the hole and the electron is indicated by the Δr index and it is found high at S2 [47].

3.8. AIM

Atoms in molecules (AIM) is a model of molecules where the main components of the molecular framework i.e., atoms as well as bonds are simple manifestations of the density of electrons of a system [48]. The features of the atom are explained by the theory of quantum physics. Based on the topology, the path of the bond and the order they indicate simply mimic and conveniently summarise the atom's activity. Fig. 9 [49] displays the topographical parameters of 5BNA. In terms of topographical studies, the critical points (CP) are locations wherein $\nabla\rho \cdot \vec{n} = 0$ [50]. The orange, magenta and yellow circles represent the CPs at the bond, nucleus and ring of the molecule. ρ (Electron density) and ∇ρ (Laplacian electron density) contribute to determining the interaction types and are tabulated in Table 7. The $\nabla^2\rho > 0$ and $\nabla^2\rho < 0$ indicate stronger and weaker hydrogen bonds. The positive $\nabla^2\rho$ values are attributed to the decreasing of charge in the internuclear zone and the negative $\nabla^2\rho$ values are attributed to an increase in covalent nature [51,52]. The ρ and $\nabla^2\rho$ values at N4–C9, C8–C9, C7–C8, C6–C7 and C5–C6 indicate the increase in covalent nature and electron density, whereas O3–C10, O2–H14, C9–H13, C8–H12 and C6–H11 indicate the moderate covalent nature and electron density.

3.9. RDG, IRI and VdW surfaces

The non-covalent interaction index (NCI) is a tool for describing interactions between molecules and determining the characteristics of interactions that are weak. They are crucial in the field of chemistry and specifically in life sciences disciplines and its foundation is RDG (Reduced density gradient) [53]. The molecular interactions that are not covalent are displayed by RDG investigations and it is expressed by the relation $\mathrm{RDG}\,(r) = \frac{1}{2(3\pi^2)^{\frac{1}{3}}} \frac{|\nabla\rho(r)|}{\rho(r)^{4/3}}$ [54]. The plot between RDG and sign (λ_2) ρ provides the interaction types and their strength present in a molecule. According to Fig. 10 [55], the repulsive effect is represented by the red region, the van Der Waals effect is represented by the green region, and the strong interaction is shown by the blue region [56].

The IRI is an effective tool that may visually indicate any sort of interaction within a system of molecules. It may highlight the poor interactions as well as the chemically bonded areas. The main benefit of IRI is its ability to depict all kinds of interaction on an equal basis [57]. Multiwfn 3.7 and VMD software are used to generate the IRI isosurfaces of 5BNA. According to Fig. 11 [58], the blue region clearly demonstrates the chemically bonded portions, i.e., the aromatic ring region, whereas the red region reveals the presence of

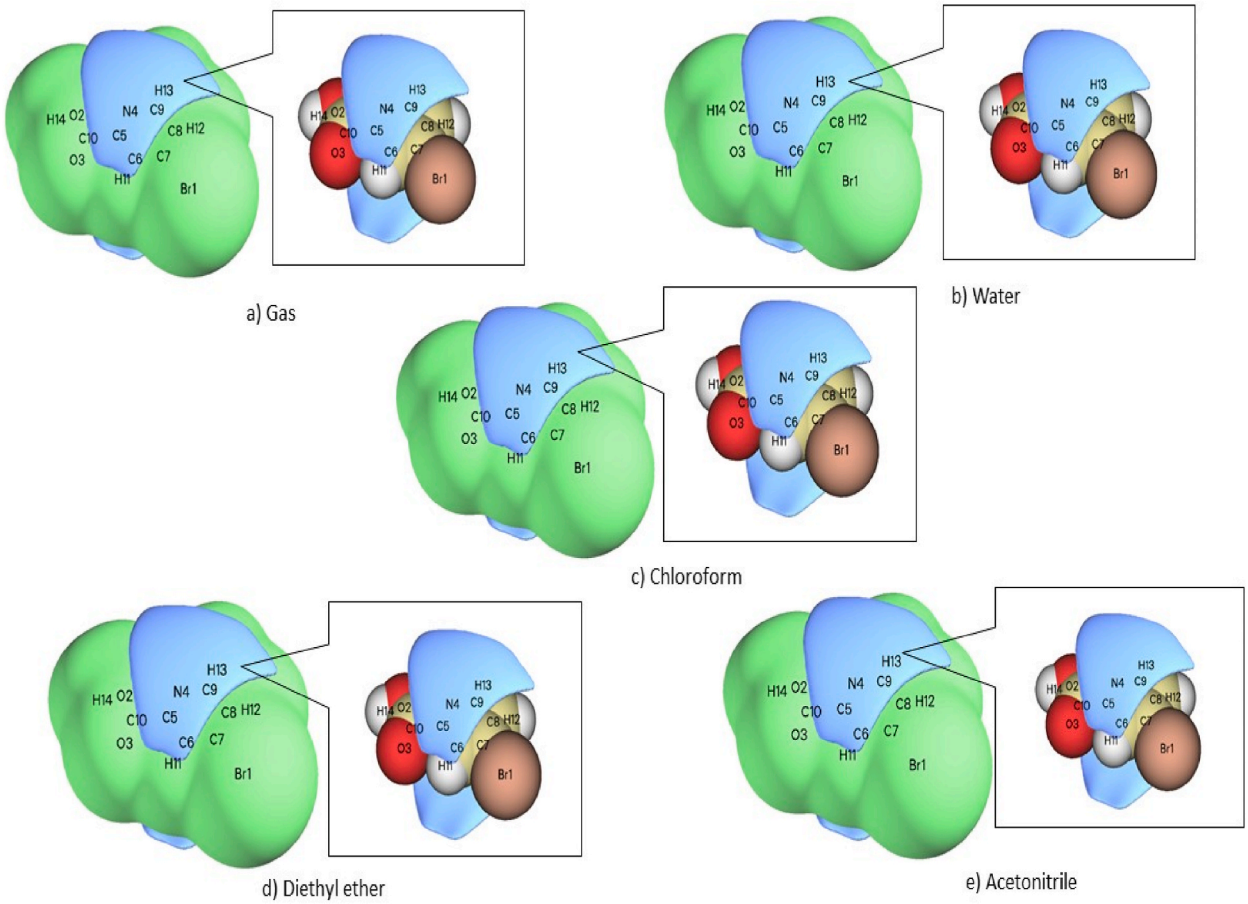

Fig. 12. Vdw isosurface of 5BNA in the a) gas phase and with different solvents media b) Water c) Chloroform d) Diethyl ether and e) Acetonitrile.

repulsiveness in the centre of the ring. Furthermore, the green region demonstrates the presence of weak contacts between the hydrogen and the oxygen atom of the carboxylic acid group. van Der Waals interactions constitute the major components of the weaker connection inside the molecules [59]. It refers to the forces of electrostatic attraction that hold molecules collectively. From Fig. 12 [60], the blue area signifies the negative zone with negative VdW potential, which is rich in the attraction effect. It is found at C5, C6, C9, N4 and H13. The green area signifies the positive zone with positive VdW potential, which signifies the repulsive zone. It is found at Br1, O2, O3, C7, C8, C10, H11, H12 and H14.

3.10. Topographical studies

ELF (Electron localization function) is used to explore the structure of a chemical molecule as it highlights the chemically important regions [61]. It gives a measure of electron localization in molecules as well as atoms because the bond and lone pairs are typically localized in certain areas of the molecule [62]. The ELF pictures were produced by the Multiwfn 3.7 application. The high ELF values of the heading molecule represent the sections of high electron-dense regions which range from 0.5 to 1.0, with a colour transition from blue to red, whereas the lowest values represent the less electron-dense region which lies in the range of 0–0.5 [63]. From Fig. 13 [64], the highest localization of electrons of 5BNA in gas as well as in the solvent phase is anticipated near the perimeter of the aromatic ring structure where the hydrogen atoms are located, whereas the delocalized electron regions are found around the carbon atoms of the aromatic ring. LOL exposes the shell structure of electrons by highlighting the localization of the innermost electrons. It is an effective technique for defining bonds between molecules. From Fig. 14 [65], the LOL map of the heading molecule ranges from 0.0 to 0.8. The blue regions have been noticed in the molecule's boundary and in the carbon atoms of the aromatic ring, indicating the weak delocalized zone containing π-orbitals. The red regions observed at the hydrogen atoms indicate a localized zone containing π-orbitals.

3.11. Electronic analysis

The UV–Visible spectrum of 5BNA in gas, water, chloroform, diethyl ether, and acetonitrile has been determined using the TD-DFT technique [66] and illustrated in Fig. 15 [67]. The absorption energy, wavelength, energy band gap and Molecular orbitals

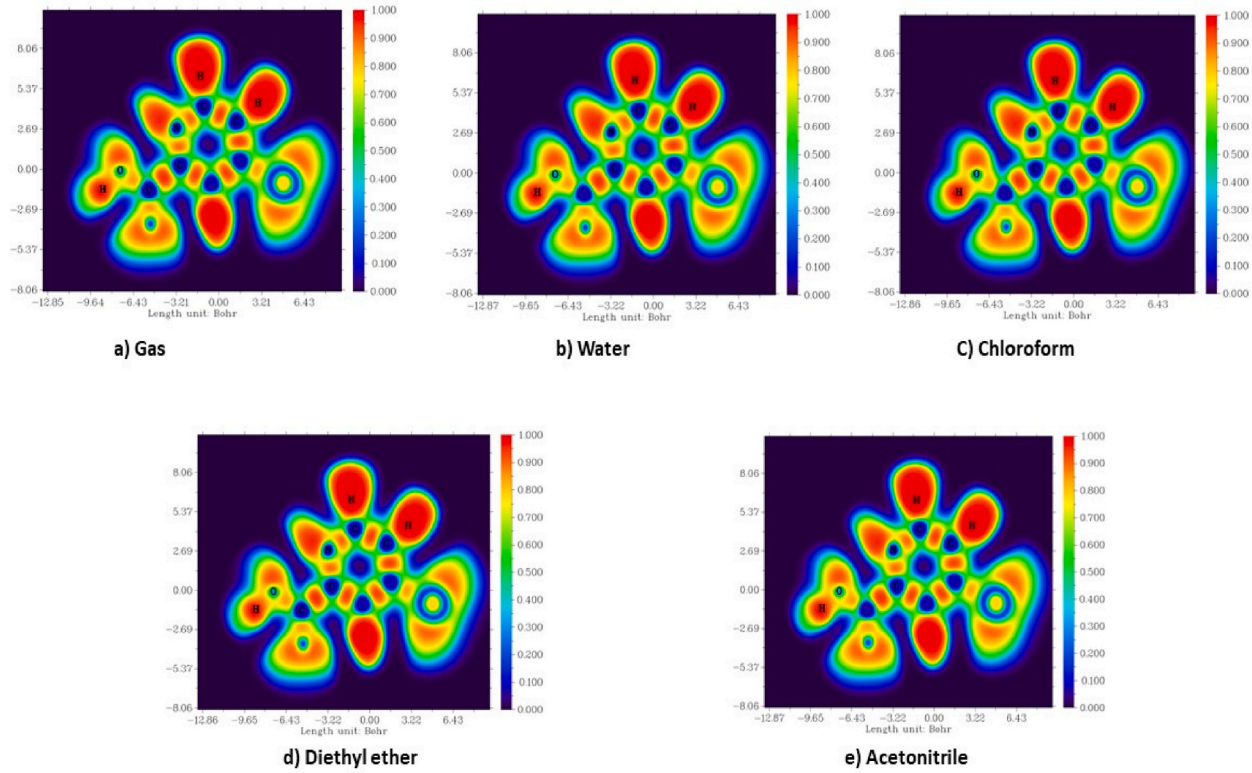

Fig. 13. ELF map of 5BNA in the a) gas phase and with different solvents media b) Water c) Chloroform d) Diethyl ether and e) Acetonitrile.

contributions are tabulated in Table 8. The impact of solvents is investigated using the IEFPCM model [68]. Between 255 and 295 nm, a broad absorbance spectrum of 5BNA in the gas phase was found. Diethyl ether has the greatest influence on the UV transition, which is followed by chloroform, acetonitrile and finally water. The highest wavelengths for gas, diethyl ether, chloroform, acetonitrile and water have been found to be 299.17 nm, 294.44 nm, 294.25 nm and 291.71 nm and 291.45 nm respectively. With the addition of solvents, there is an increase in energy as well as in the band gap of 5BNA. The electronic transitions π to π* will shift to longer wavelengths whereas, n to π* and n to σ* will shift towards the lower wavelengths when the polarity of the solvent increases. According to the absorption study, there was a slight hypochromic shift in the absorption spectra when the solvents were incorporated [69]. The shifted absorption spectra show that solvents are involved in causing the intramolecular interaction in the molecule. Furthermore, the spectral shifts were caused by the HOMO and LUMO charge cloud altering with the lowest energy [70]. Consequently, the calculated wavelengths 299.17 nm, 291.45 nm, 294.25 nm, 294.44 nm and 291.71 nm for the 5BNA in gas as well as with the solvents water, chloroform, diethyl ether and acetonitrile show the n to π* transition.

3.12. Vibrational analysis

The heading molecule comprises 14 atoms with 36 modes of vibrations. The spectra base site is utilised to obtain experimental FT-IR and FT-Raman spectra and the obtained results are compared with the theoretical results obtained from the computational approach (Figs. 16 and 17) [71,72]. For 5BNA, there were minor differences in frequency between the theoretical and experimental spectra because the experimental spectra were obtained in solid form, whereas the theoretical spectra were observed in the gas and solvent phases (Table 9). PED analysis allows for the possibility of numerically defining each mode's characteristics by expressing the relative contributions of the redundant internal coordinates to each of the molecule's typical vibrational modes [73].

C–H vibrations are often detected in 3100 to 3000 cm^{-1} range [74]. For 5BNA the C–H stretching is observed at 3098, 3084, and 3036 cm^{-1}. In experimental FTIR and FT Raman, they are observed at 3010 and 3599 cm^{-1}. For mixed-mode H–C–C bending it is observed at 1538, 1434, 1369, 1316, 1076 and 1058 cm^{-1}. The mixed-mode bending vibrations is noticed in the experimental FTIR at 1615 and 1394 cm^{-1} and FT Raman are observed at 1566, 1502, 1438, 1348 and 1004 cm^{-1}. Torsional vibrations of H–C–C–C are recorded at 900 and 770 cm^{-1}.

C–C vibrations are often detected in 1650 to 1100 cm^{-1} range [75]. For this compound, it is seen at 1538, 1527, 1434, 1369, 1255, 1236, 1167, 1076, 1058, 969, 794, 770 and 379 cm^{-1}. In experimental FTIR and FT Raman, they are observed at 1528 and 1502 cm^{-1}. The mixed-mode C–C–C bending vibrations are noticed at 969, 665 and 292 cm^{-1}. In experimental FTIR it is observed at 673 cm^{-1}.

O–H vibrations are often detected in the 3700 to 3100 cm^{-1} range [76]. For this compound, it is seen at 3615 cm^{-1}. In experimental

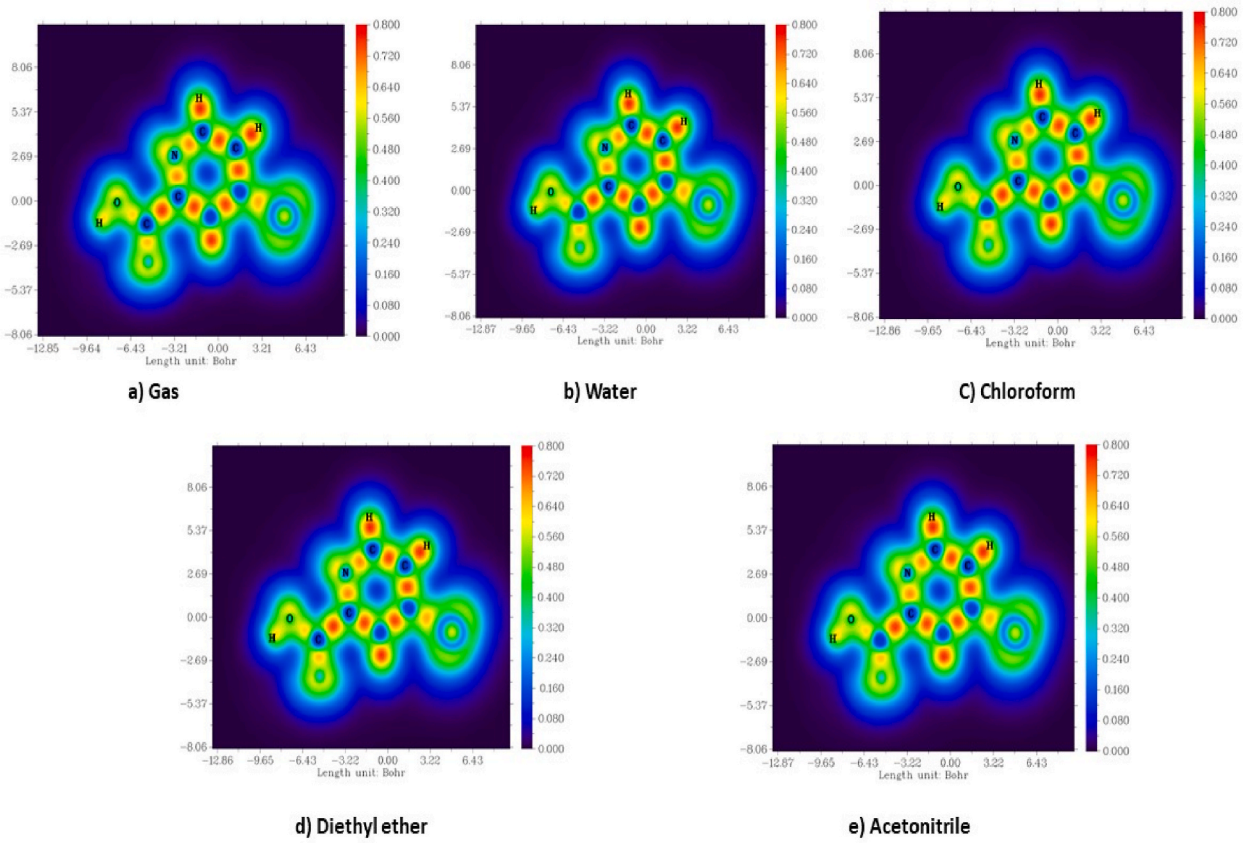

Fig. 14. LOL map of 5BNA in the a) gas phase and with different solvents media b) Water c) Chloroform d) Diethyl ether and e) Acetonitrile.

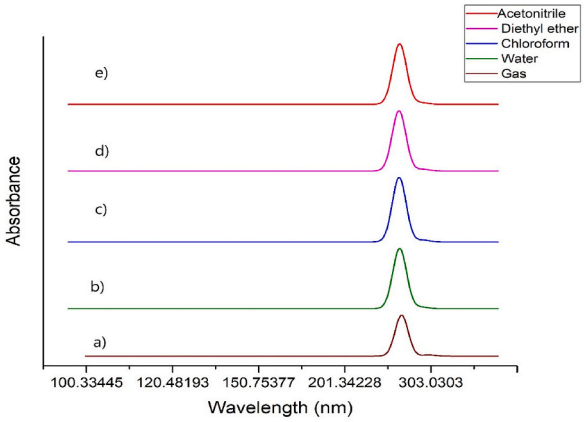

Fig. 15. UV–Vis spectra of 5BNA in the a) gas phase and with different solvents media b) Water c) Chloroform d) Diethyl ether and e) Acetonitrile.

FTIR and FT Raman, they are observed at 3445 and 3601 cm^{-1}. The mixed-mode H–*O*–C bending vibrations are observed at 1316 and 1167 cm^{-1}. The experimental mixed-mode bending vibrations are noticed in FTIR at 1115 cm^{-1}. The torsional vibrations of H–*O*–C–C are observed at 585, 697, 585, 485, 403 and 131 cm^{-1}.

O–C vibrations are often detected in 1320 to 1000 cm^{-1} range [77]. For this, it is seen at 1316, 1093 and 1076 cm^{-1}. C═O vibrations are detected at 1710 to 1680 cm^{-1} [78]. The C═O vibration for 5BNA is noticed at 1714 cm^{-1}. In experimental FTIR and FT Raman, they are noticed at 1615 and 1655 cm^{-1}.

C-X (Br) vibrations are observed in the region of 300–800 cm^{-1} [79]. For this compound, the Br–C stretching is observed at 665, 292 and 258 cm^{-1}. The experimental FTIR is observed at 673 cm^{-1}. The mixed bending vibrations for C–C–Br bending are 292 and 258

Table 8
Electronic parameters of 5BNA in the gas phase and with various solvent media.

Solvents	Energy (cm^{-1})	Wavelength (nm)	Osc. Strength	Band gap (eV)	Major Contributions
Gas	33426.0352	299.17	0.0009	4.14	HOMO- > LUMO (99%)
	38705.74049	258.36	0.0285	4.80	H-2- > L+1 (10%), H-1- > LUMO (79%)
	38977.54934	256.56	0.0007	4.83	H-4- > LUMO (24%), H-3- > LUMO (59%), HOMO- > L+1 (14%)
Water	34311.63196	291.45	0.0012	4.25	H-1- > LUMO (99%)
	38304.07639	261.07	0.0427	4.75	HOMO- > LUMO (80%)
	39871.21164	250.81	0.0006	4.94	H-4- > LUMO (71%), H-3- > LUMO (19%)
Chloroform	33984.17087	294.25	0.0013	4.21	H-1- > LUMO (99%)
	38394.41048	260.45	0.0456	4.76	HOMO- > LUMO (80%)
	39598.59625	252.53	0.0007	4.91	H-4- > LUMO (63%), H-3- > LUMO (24%), H-1- > L+1 (10%)
Diethyl ether	33963.20045	294.44	0.0012	4.21	H-1- > LUMO (99%)
	38427.47922	260.23	0.0425	4.77	HOMO- > LUMO (80%)
	39582.46516	252.64	0.0007	4.91	H-4- > LUMO (61%), H-3- > LUMO (25%), H-1- > L+1 (10%)
Acetonitrile	34280.9829	291.71	0.0012	4.25	H-1- > LUMO (99%)
	38312.14193	261.01	0.043	4.75	HOMO- > LUMO (80%)
	39847.82156	250.95	0.0006	4.94	H-4- > LUMO (70%), H-3- > LUMO (19%)

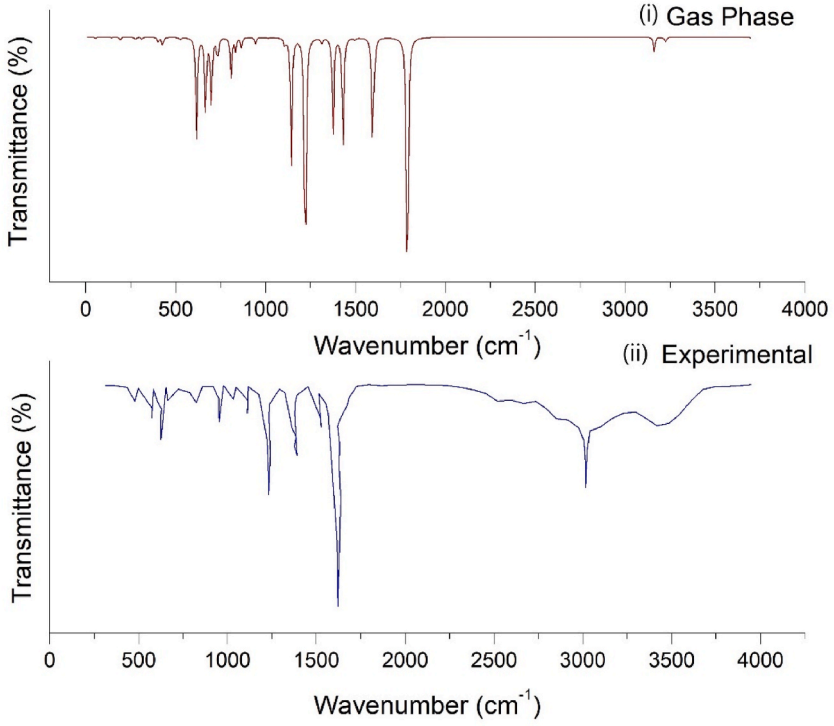

Fig. 16. Compared (i) Gas phase and (ii) Experimental FTIR spectrum of 5BNA.

cm^{-1}. The other vibrations such as out-of-plane vibrations for C–C–N–C are at 900 and 770 cm^{-1} and for O–C–C–C is noticed at 44 cm^{-1}.

3.13. Biological analysis

In order to increase the likelihood of a chemical substance accessing and succeeding in clinical investigations, the idea of drug-likeness was put up as valuable guidance during the early phases of drug research [80]. It is established through the biophysical and biochemistry scientific research on emerging compounds that have advanced sufficiently to be considered as medicine taken as oral alternatives. The rule of five proposed by Lipinski is widely employed to predict the probability that a compound will have dominant drug-like characteristics and therefore qualify as a successful pharmaceutical applicant [81]. From Table 10, in 5BNA, the rotatable bonds present is 1 ($\geq$ 10), the H bond acceptor and donor are 3 ($\geq$ 10) and 1 ($\geq$ 5), the TPSA (Topological polar surface area) is 50.19 $Å^2$ (40–130 $Å^2$) and AlogP is 1.54 (0.4–5.6). The compound 5BNA satisfies Lipinski's rule. This compound is extremely soluble in water, as indicated by a solubility score (log S) of less than −2. Furthermore, a BBB (blood-brain barrier) score of less than 5 signifies

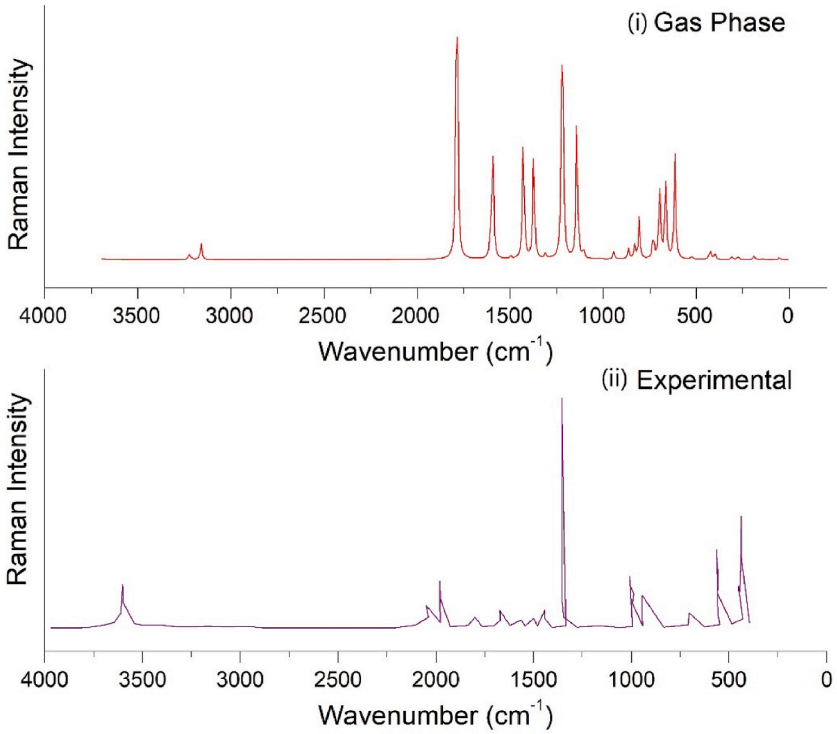

Fig. 17. Compared (i) Gas phase and (ii) Experimental FT-Raman spectrum of 5BNA.

that the substance is known as a non-CNS (Central nervous system) medication. The lead-like criterion is followed and there are no violations, however, the compound is only appropriate if its binding affinity is more than 0.1 μM. The pharmacologic filters PAINS and Brenk are implemented to identify drugs that have poor physicochemical characteristics and this compound shows zero violation indicating that there is no false occurrence of positives and is suggested to be used in Insilco drug discovery [82]. The bioavailability score of 0.85 provides the validation for the compound as an orally absorbable drug.

The complementary approach by Insilco prediction methods aims to optimise the preclinical drug discovery technique in an attempt to reduce the time, expense and involvement of animals. Using computational modelling for the drug development process offers many advantages [83]. The ProTox II webserver has been utilised to test the chemical compound's toxicity. The prediction technique represents an original strategy in toxicology prediction because it combines the recognition of toxic components and is based on the comparison of substances with reported average lethal doses (LD50) [84]. The compound 5BNA is not carcinogenic, cytotoxic, immunotoxin and mutagenic. Moreover, it does not cause p53 gene (tumour suppressor) mutation along with the inactive Heat shock response. The average lethal dosage (LD50) for 5BNA is predicted to be 3720 mg/kg and it lies in the toxicity class of Class VI which indicates that the compound is non-toxic in nature and can also be proposed as the drug [85].

3.14. Hydropathy and Ramachandran plot

A molecule may be either apprehensive of water (hydrophobic) or attracted to water (hydrophilic). One aspect that affects the structure of a molecule is its hydropathy. Hydropathy plots illustrate the degree of hydrophobicity of a polypeptide chain over its whole length. It serves as the centre of attention in investigating the folding of proteins and steadiness, especially in both inner and outer areas, antigen spots, etc [86]. Expasy web server is used to obtain the hydropathy plot (Kyte-Doolittle) of the protein [87]. Fig. 18 [88] illustrates the hydropathy plots of proteins 2A4O, 6CWD and 2OC8. The negative peaks on the plot indicate the amino acid which is hydrophobic and they lie inside the protein. Whereas, the positive peaks indicate the amino acids which are hydrophilic and they lie outside the protein [89]. From Table S2, the maximum hydrophobicity is found for the amino acid isoleucine (ILE:4.5) and the maximum hydrophilicity is found for the amino acid lysine (LYS:3.9) [90].

The Ramachandran plot has been used for the proteins which are selected for the docking investigations with the help of the PDBSum web server [91]. This plot is also called the φ and ψ (torsion angles) plot of the residues of amino acids present in the protein. It entails charting the φ and ψ values on the x and y axis to estimate the protein's potential structure. From -180° to $+180^{\circ}$ is the range of angles along each of the axes [92]. From Fig. 19 [93], the red and brown patches constitute the allowed and permitted zones of the amino acids. The red patches correspond to the steric hindrance. These patches comprise beta-sheet and alpha helix. Thus, the amino acid residues of the selected proteins 2A4O, 6CWD and 2OC8 lie within the permitted limited.

Table 9
Vibrational assignments of 5BNA in the gas phase and with various solvent media.

Experimental FT-IR[a]	Experimental FT-Raman[b]	Gas	Water	Chloroform	Diethyl ether	Acetonitrile	Vibrational Assignments*
3445	3601	3615	3596	3602	3603	3597	γOH(100)
	3599	3098	3103	3101	3100	3102	γCH(99)
3010	2045	3084	3092	3089	3089	3092	γCH(97)
2856	1801	3036	3048	3045	3043	3048	γCH(97)
1615	1665	1714	1679	1689	1691	1680	γOC(85)
	1566	1538	1535	1536	1537	1536	γCC(67)+βHCC(10)
1528	1502	1527	1526	1526	1526	1526	γCC(50)
	1438	1434	1434	1434	1435	1434	γCC(22)+βHCC(47)
1394	1348	1369	1367	1368	1368	1367	γCC(13)+βHCC(21)+βCNC(11)
		1316	1309	1312	1312	1309	γOC(14)+βHOC(26)+βHCC(10)+βCNC (11)
		1255	1254	1254	1254	1254	γCC(14)+βHCC(59)
1230		1236	1237	1236	1237	1237	γCC(85)
1115		1167	1160	1161	1161	1160	γCC(11)+βHOC(38)
		1093	1085	1087	1087	1085	γOC(39)+βCNC(10)
		1076	1077	1077	1077	1077	γCC(19)+γOC(12)+βHCC(41)+βCNC (11)
1028	1004	1058	1057	1057	1057	1057	γCC(42)+βHCC(41)+βCNC(11)
		969	969	969	969	969	γCC(36)+βCCC(47)
952	941	953	960	958	958	960	τHCNC(66)+τCCCN(21)
		900	894	896	896	894	τHCCC(75)+ωCCNC(10)
827		825	830	829	829	830	τHCCN(79)
		794	792	793	793	792	γOC(13)+γCC(21)+βCNC(31)
		770	769	769	769	769	τHCCC(11)+τHCCN(11)+ωCCNC(70)
	697	697	694	695	695	694	τHCNC(12)+τHOCC(69)
673		665	662	662	663	662	γBrC(19)+βCCC(49)
625		634	628	629	629	628	βCNC(57)
577	561	585	571	574	574	572	τHOCC(88)
		497	499	498	498	499	βCCO(71)
471	471	485	484	484	483	484	τHOCC(60)+τCCNC(11)
		403	404	404	403	404	τHOCC(15)+βHCNC(11)+τCCCN(55)
		379	381	380	380	381	γCC(30)+βCNC(50)
		292	292	292	292	292	γBrC(39)+βCCC(10)+βCCBr(31)
		258	262	260	259	262	γBrC(20)+βCCBr(55)
		176	177	176	176	177	ωCCNC(81)
		131	133	132	132	133	τHOCC(23)+ωCCNC(60)
		131	133	131	131	132	βCCBr(78)
		44	44	41	40	43	ωOCCC(90)

**γ - stretching, β - in-plane bending, τ - out-plane bending and ω - torsion.
[a] SpectraBase Spectrum ID: C5xjMI0FFTw.
[b] SpectraBase Spectrum ID: FgEEb9bmsM9.

Table 10
Drug likeness and Toxicity parameters of 5BNA.

Parameters	Value
Hydrogen bond Donor (HBD)	1
Hydrogen bond Acceptor (HBA)	3
A LogP	1.54
Topological polar surface area (TPSA)	50.19
Molar refractivity	38.9
Number of atoms	13
Number of rotatable bonds	1
BBB	0.9
LogS	−1.72
Bioavailability Score	0.85
PAINS	0
Brenk	0
Carcinogenicity	Inactive
Immunotoxicity	Inactive
Mutagenicity	Inactive
Cytotoxicity	Inactive
P50	Inactive
Heat shock response	Inactive
LD50	3720 mg/kg

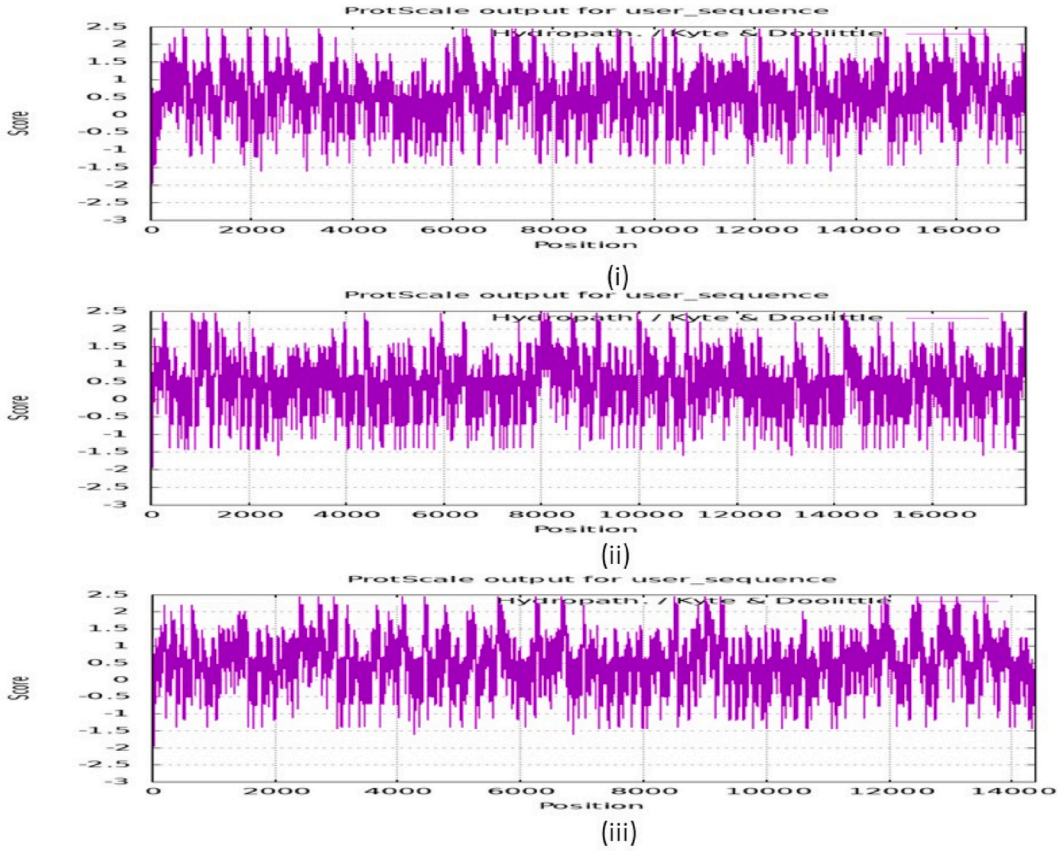

Fig. 18. Hydropathy plot of the proteins (i) 2A4O, (ii) 6CWD and (iii) 2OC8.

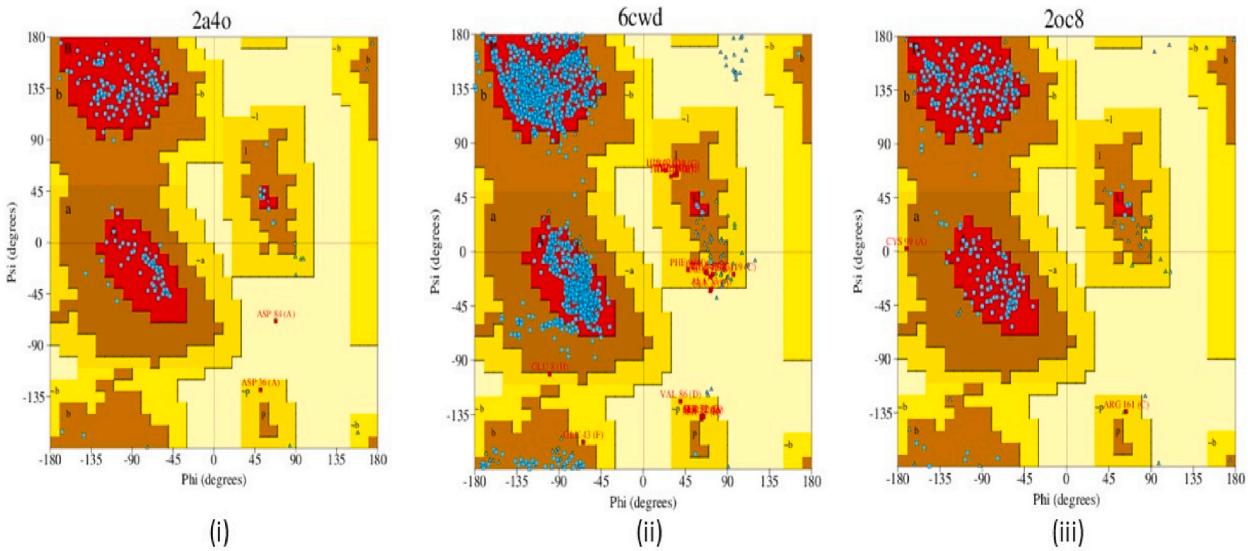

Fig. 19. Ramachandran plot of the proteins (i) 2A4O, (ii) 6CWD and (iii) 2OC8.

3.15. Insilco drug designing

Molecular docking has evolved into a significant part of the drug development technique. Using the PASS analysis tool, the antiviral activity especially for Hepatitis is predicted. Hepatitis is a communicable viral infection. It causes an infection in the liver by causing

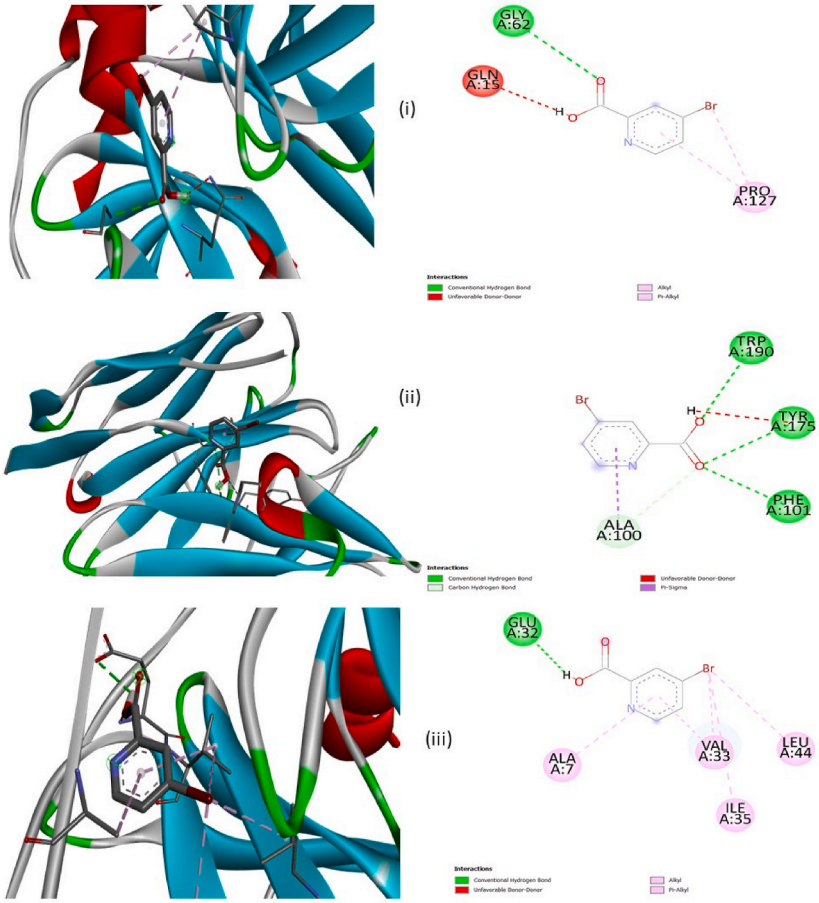

Fig. 20. Proteins (i) 2A4O, (ii) 6CWD and (iii) docked with the ligand 5BNA.

Table 11
Molecular docking parameters of protein 2A4O, 6CWD and 2OC8 docked with 5BNA.

PDB ID	Binding energy (kcal/mol)	Intermolecular Energy (kcal/mol)	Bonded Residues	Bond Distance (Å)	Bond Type	Interaction Type
2A4O	−4.7	−5	GLY62	3.17	Hydrogen Bond	Conventional Hydrogen Bond
			PRO127	4.54	Hydrophobic	Alkyl
			PRO127	5.41	Hydrophobic	Pi-Alkyl
6CWD	−5.3	−5.6	PHE101	3.12	Hydrogen Bond	Conventional Hydrogen Bond
			TYR175	3.08	Hydrogen Bond	Conventional Hydrogen Bond
			TRP190	2.98	Hydrogen Bond	Conventional Hydrogen Bond
			ALA100	3.44	Hydrogen Bond	Carbon Hydrogen Bond
2OC8	−5.2	−5.5	GLU32	2.55	Hydrogen Bond	Conventional Hydrogen Bond
			VAL33	4.80	Hydrophobic	Alkyl
			ILE35	4.74	Hydrophobic	Alkyl
			LEU44	4.31	Hydrophobic	Alkyl
			ALA7	5.00	Hydrophobic	Pi-Alkyl
			VAL33	4.69	Hydrophobic	Pi-Alkyl

damage to liver tissues [94]. The PDB files of the proteins 2A4O, 6CWD and 2OC8 are obtained from the RCSB PDB server and they are associated with Hepatitis A, Hepatitis B and Hepatitis C [95]. The Autodock Vina utility in the PyRx application uses the Lamarckian algorithm and empirical energy score model for pliable ligand and protein receptor docking [96]. The Chain A of the protein 2A4O,

6CWD and 2OC8 is selected along with its active site for the docking. The grid centre with dimensions (x, y and z) for the protein 2A4O is 0.455 points, 14.668 points and 31.700 points with a volume of 313 $Å^3$, for 6CWD it is 145.664 points, −60.848 points and 317.057 points with the volume of 141 $Å^3$ and for 2OC8 it is 198.890 points, −4.387 points and 50.450 points with the volume of 152 $Å^3$ [97, 98]. The visualisation of protein and ligand sites is done using the PyRx and BIOVIA Discovery Studio applications. The proteins 2A4O, 6CWD and 2OC8 docked with the ligand 5BNA are displayed in Fig. 20 [99]. The distances between associated residues of amino acids, category of bond, binding energy and interaction energy are listed in Table 11. In common, the bond type observed between the ligand and the amino acid residues is a hydrogen and hydrophobic bond. With the ligand 5BNA, the interacted of amino acid residues of the protein 24AO are GLY62 with conventional H bond, PRO127 with alkyl interaction and PRO127 with pi-alkyl interaction, for the protein 6CWD, the interacted of amino acid residues are PHE101, TYR175 and TRP 190 with conventional H bond and ALA100 with C–H bond and for the protein 2OC8 the interacted of amino acid residues are GLU32, VAL33 and ILE35 with alkyl interaction and ALA7 and VAL33 with pi-alkyl interaction. The negative values of the binding energy signify the exhibition of activity against Hepatitis [100].

4. Conclusion

The DFT approach is employed to theoretically characterize the structural and electronic characteristics of 5-Bromonicotinatic acid by using different organic solvents. The various reactive and fingerprint zones present in the compound are picturised using the ESP map, Fukui analysis and Hirshfeld surface. μ, α and β of 5BNA exhibit a shift when they switch between the gas to the solution phases. Through the NBO analysis, the highest stabilisation energy of 47.29 kcal/mol is found for the transition between the LP O2→ π* O3–C10. In 5BNA, the majority of transitions occur between the π and π*. The molecular orbital energy difference of 5BNA with the diethyl ether has the highest energy difference of 5.46522eV compared with other solvents and gas phase of 5BNA. The highest values of the D index i.e., <1 and the H index indicate the presence of charge transfer within the molecule. The highest values of ρ and $\nabla^2\rho$ by AIM analysis at the N4–C9, C8–C9, C7–C8, C6–C7 and C5–C6, indicate that the 5BNA in both gas phase as well as with solvent show maximum electron density and covalent nature. By ELF and LOL studies, the electron dense region is found at the circumference of the aromatic ring and the electron-deficit zone is found at the carbon atoms. By the UV–Vis spectra, the maximum absorption wavelength is observed at 299.17 nm for gas and 294.44 nm for diethyl ether. The various molecular vibrations present in the compound are determined and documented using vibrational spectroscopy (IR and Raman) and their wavenumbers are correlated with the experimental values. 5BNA's drug-likeness and toxicity effects show that compound 5BNA can be suggested as a drug. The proteins 2A4O, 6CWD and 2OC8 associated with Hepatitis A, Hepatitis B and Hepatitis C are docked with the ligand 5BNA and has the binding energy of −4.7 kcal/mol, −5.3 kcal/mol and −5.2 kcal/mol.

Author contribution statement

Sravanthi R: Conceived and designed the experiments; Performed the experiments; Analyzed and interpreted the data; Wrote the paper.

S Mahalakshmi: Performed the experiments; Analyzed and interpreted the data; Wrote the paper.

S Kumaran; Shine Kadaikunnan: Analyzed and interpreted the data.

Ghulam Abbas: Contributed reagents, materials, analysis tools or data; Analyzed and interpreted the data.

S Muthu: Conceived and designed the experiments; Contributed reagents, materials, analysis tools or data.

Data availability statement

Data will be made available on request.

Declaration of competing interest

The authors declare that they have no known competing financial interests or personal relationships that could have appeared to influence the work reported in this paper.

Acknowledgement

The authors express their sincere appreciation to the Researchers Supporting Project Number (RSPD2023R696), King Saud University, Riyadh, Saudi Arabia.

Appendix A. Supplementary data

Supplementary data to this article can be found online at https://doi.org/10.1016/j.heliyon.2023.e19965.

References

[1] E. Vaganova, D. Eliaz, U. Shimanovich, G. Leitus, E. Aqad, V. Lokshin, V. Khodorkovsky, Light-induced reactions within poly(4-vinyl pyridine)/pyridine gels, The 1,6-Polyazaacetylene Oligomers Formation 26 (22) (2021) 6925.

[2] Role of Pyridines in Medicinal Chemistry and Design of BACE1 Inhibitors Possessing a Pyridine Scaffold, Yoshio Hamada, 2018, https://doi.org/10.5772/intechopen.74719.

[3] Xolani Henry Makhoba, Chapter 5 - the role of pyridine derivatives on the treatment of some complex diseases: a review, Recent Developments in the Synthesis and Applications of Pyridines (2023) 143–158, https://doi.org/10.1016/B978-0-323-91221-1.00015-4.

[4] Henri A. Favre, Warren H. Powell, Chapter P-6, applications to specific classes of compounds, Nomenclature of Organic Chemistry 648–1047 (2013), https://doi.org/10.1039/9781849733069-00648.

[5] D. Laudert, H.-P. Hohmann, 3.50 - Application of Enzymes and Microbes for the Industrial Production of Vitamins and Vitamin-like Compounds, Comprehensive Biotechnology, 2011, pp. 616–634, https://doi.org/10.1016/B978-0-444-64046-8.00188-9.

[6] John E. Halver, Chapter 10 - nutrition of salmonids, developments in aquaculture and fisheries, Science ume 29 (1996) 613–653, https://doi.org/10.1016/S0167-9309(96)80013-5.

[7] Edward Behrman, R. Stanier, Oxidation of halogenated nicotinic acids, J. Biol. Chem. 228 (1957) 947–953, https://doi.org/10.1016/S0021-9258(18)70672-8.

[8] M. Vennila, R. Rathikha, S. Muthu, A. Jeelani, Irfan Ahmad, Theoretical structural analysis (FT-IR, FT-R), solvent effect on electronic parameters NLO, FMO, NBO, MEP, UV (IEFPCM model), Fukui function evaluation with pharmacological analysis on methyl nicotinate, Computational and Theoretical Chemistry 1217 (2022), 113890, https://doi.org/10.1016/j.comptc.2022.113890.

[9] S. Sarala, S.K. Geetha, S. Muthu, Irfan Ahmad, Probing solvent effect and strong and weak interactions in 2-Nitrophenyl-hydrazine using independent gradient model and Hirshfeld from wave function calculation, J. Mol. Liq. 341 (2021), 117345, https://doi.org/10.1016/j.molliq.2021.117345.

[10] Sheryl Cherian Parakkal, Riya Datta, A. Saral, S. Muthu, Irfan Ahmad, A. Jeelani, Solvent polarity, structural and electronic properties with different solvents and biological studies of 3,3,5-triphenylfuran-2(3H)-one- cancers of the blood cells 368 (2022), 120674, https://doi.org/10.1016/j.molliq.2022.120674. Part B.

[11] C. Narth, et al., A complete NCI perspective: from new bonds to reactivity, in: R. Chauvin, C. Lepetit, B. Silvi, E. Alikhani (Eds.), Applications of Topological Methods in Molecular Chemistry. Challenges and Advances in Computational Chemistry and Physics, vol. 22, Springer, Cham, 2016, https://doi.org/10.1007/978-3-319-29022-5_18.

[12] M.J. Frisch, G.W. Trucks, H.B. Schlegel, et al., Gaussian 09, Revision A.02, Gaussian, Inc., Wallingford, CT, USA, 2009.

[13] Ksg Dennington, Roy, Todd A. Keith, John M. Millam, Semichem inc., shawnee mission, Gaussview 6 (2016).

[14] M.H. Jamróz, Vibrational energy distribution analysis (VEDA): scopes and limitations, Spectrochim. Acta Mol. Biomol. Spectrosc. 114 (2013 Oct) 220–230, https://doi.org/10.1016/j.saa.2013.05.096.

[15] Tian Lu, Feiwu Chen, Multiwfn, A multifunctional wavefunction analyzer, J. Comput. Chem. 33 (2012) 580–592, https://doi.org/10.1002/jcc.22885.

[16] SwissADME, A free web tool to evaluate pharmacokinetics, drug-likeness and medicinal chemistry friendliness of small molecules, Sci. Rep. 7 (2017), 42717.

[17] GUSAR - Prediction of Values for Substances Copyright (C), A. Zakharov, V. Poroikov & Associates, 2010. http://pharmaexpert.ru/GUSAR/environmental.html.

[18] M.N. Drwal, P. Banerjee, M. Dunkel, M.R. Wettig, R. Preissner, ProTox: a web server for the in silico prediction of rodent oral toxicity, Nucleic Acids Res. 42 (2014 Jul). Web Server issue): W53-8.

[19] S. Dallakyan, A.J. Olson, Small-molecule library screening by docking with PyRx, Methods Mol. Biol. 1263 (2015) 243–250, https://doi.org/10.1007/978-1-4939-2269-7_19.

[20] BIOVIA, Dassault Systèmes, [Discovery Studio], 2021, Dassault Systèmes, San Diego, 2021.

[21] T. Sasitha, W.J. John, Design, docking, and DFT investigations of 2,6-bis(3,4-dihydroxyphenyl)-3-phenethylpiperidin-4-one, Heliyon 7 (2) (2021 Feb 11), e06127, https://doi.org/10.1016/j.heliyon.2021.e06127.

[22] C.B. Aakeroy, A.M. Beatty, M. Tremayne, D.M. Rowe, C.C. Seaton, CCDC 172544: Experimental Crystal Structure Determination, 2002, https://doi.org/10.5517/cc5sjyd.

[23] Modesto Orozco, Francisco J. Luque, Generalization of the molecular electrostatic potential for the study of noncovalent interactions, Theoretical and Computational Chemistry 3 (1996) 181–218, https://doi.org/10.1016/S1380-7323(96)80044-6.

[24] Benjamin G. Janesko, Density functional theory for transition metal catalysis, reference module in chemistry, Molecular Sciences and Chemical Engineering (2022), https://doi.org/10.1016/B978-0-12-821978-2.00015-5.

[25] Olfa Noureddine, Noureddine Issaoui, Mouna Medimagh, Omar Al-Dossary, Houda Marouani, Quantum chemical studies on molecular structure, AIM, ELF, RDG and antiviral activities of hybrid hydroxychloroquine in the treatment of COVID-19: molecular docking and DFT calculations, J. King Saud Univ. Sci. 33 (Issue 2) (2021), 101334, https://doi.org/10.1016/j.jksus.2020.101334.

[26] Apoorva Dwivedi, Vikas Baboo, Abhishek Bajpa, Fukui function analysis and optical, electronic, and vibrational properties of tetrahydrofuran and its derivatives: a complete quantum chemical study, Journal of Theoretical Chemistry 2015 (2015), 345234, https://doi.org/10.1155/2015/345234.

[27] Weitao Yang, Wilfried J. Mortier, The use of global and local molecular parameters for the analysis of the gas-phase basicity of amines, Am. Chem. Soc. 108 (19) (1986) 5708–5711, https://doi.org/10.1021/ja00279a008.

[28] Jorge Martínez-Araya, Why is the dual descriptor a more accurate local reactivity descriptor than Fukui functions? J. Math. Chem. 53 (2014) https://doi.org/10.1007/s10910-014-0437-7.

[29] L.J. Barbour, 2.03 - Single-Crystal X-Ray Diffraction, Comprehensive Supramolecular Chemistry II, 2017, pp. 23–43, https://doi.org/10.1016/B978-0-12-409547-2.12493-X.

[30] Kadri Rayene, Djellala Imane, Bouhadiba Abdelaziz, Nouar Leila, Madi Fatiha, Guendouzi Abdelkrim, Gassoumi Bouzid, Lafifi Ismahan, Houari Brahim, Oumeddour Rabah, Molecular modeling study of structures, Hirschfield surface, NBO, AIM, RDG, IGM and 1HNMR of thymoquinone/hydroxypropyl-β-cyclodextrin inclusion complex from QM calculations, J. Mol. Struct. 1249 (2022), 131565, https://doi.org/10.1016/j.molstruc.2021.131565.

[31] V. Jevtović, H. Hamoud, S. Al-Zahrani, K. Alenezi, S. Latif, T. Alanazi, F. Abdulaziz, D. Dimić, Synthesis, crystal structure, quantum chemical analysis, electrochemical behavior, and antibacterial and photocatalytic activity of Co complex with pyridoxal-(S-Methyl)-isothiosemicarbazone ligand, Molecules 27 (15) (2022) 4809, https://doi.org/10.3390/molecules27154809.

[32] Ikram Jomaa, Olfa Noureddine, Sofian Gatfaoui, Noureddine Issaoui, Thierry Roisnel, Houda Marouani, Experimental, computational, and in silico analysis of (C8H14N2)2[CdCl6] compound, J. Mol. Struct. 1213 (2020), 128186, https://doi.org/10.1016/j.molstruc.2020.128186.

[33] J. Jens Wolff, Rüdiger Wortmann, Organic materials for second-order non-linear optics, in: s), D. Bethell (Eds.), Advances in Physical Organic Chemistry, vol. 32, Academic Press, 1999, pp. 121–217, https://doi.org/10.1016/S0065-3160(08)60007-6.

[34] Elsa Garmire, Nonlinear optics in daily life, Opt Express 21 (2013) 30532–30544, https://doi.org/10.1364/OE.21.030532.

[35] Ireshika C. de Silva, Rohini M. de Silva, K.M. Nalin de Silva, Investigations of nonlinear optical (NLO) properties of Fe, Ru and Os organometallic complexes using high accuracy density functional theory (DFT) calculations, J. Mol. Struct.: THEOCHEM 728 (2005) 141–145, https://doi.org/10.1016/j.theochem.2005.02.092. Issues 1–3.

[36] C. Rathika Thaya Kumari, M. Nageshwari, R. Ganapathi Raman, M. Lydia Caroline, Crystal growth, spectroscopic, DFT computational and third harmonic generation studies of nicotinic acid, J. Mol. Struct. 1163 (2018) 137–146, https://doi.org/10.1016/j.molstruc.2018.02.091.

[37] A. Shiroudi, Z. Safaei, Z. Kazeminejad, E. Repo, K. Pourshamsian, DFT study on tautomerism and natural bond orbital analysis of 4-substituted 1,2,4-triazole and its derivatives: solvation and substituent effects, J. Mol. Model. 26 (3) (2020 Feb 13) 57, https://doi.org/10.1007/s00894-020-4316-9.

[38] P. Venkata Ramana, Sundius Tom, S. Muthu, K. Chandra Mouli, Y. Rama Krishna, K. Venkata Prasad, R. Niranjana Devi, Irfan Ahmad, C. Santhamma, Spectroscopic, quantum mechanical, electronic excitation properties (Ethanol solvent), DFT investigations and molecular docking analysis of an anti-cancer drug Bendamustine, J. Mol. Struct. 1253 (2022), 132211, https://doi.org/10.1016/j.molstruc.2021.132211.

[39] Christina Susan Abraham, S. Muthu, Johanan Christian Prasana, B. Fathima Rizwana, Stevan Armaković, Sanja J. Armaković, Vibrational and electronic absorption spectroscopic profiling, natural hybrid orbital, charge transfer, electron localization function and molecular docking analysis on 3-amino-3-(2-nitrophenyl) propionic acid, J. Mol. Struct. 1171 (2018) 733–746, https://doi.org/10.1016/j.molstruc.2018.06.057.

[40] A.R. Oliaey, A. Shiroudi, E. Zahedi, et al., Theoretical study on the mechanisms and kinetics of the β-elimination of 2,2-dihaloethyltrihalosilanes (X = F, Cl, Br) compounds: a DFT study along with a natural bond orbital analysis, React. Kinet. Mech. Catal. 124 (2018) 27–44, https://doi.org/10.1007/s11144-017-1332-6.

[41] Benjamin D. Dunnington, J.R. Schmidt, Generalization of natural bond orbital analysis to periodic systems: applications to solids and surfaces via plane-wave density functional theory, J. Chem. Theor. Comput. 8 (6) (2012) 1902–1911, https://doi.org/10.1021/ct300002t.

[42] Sofian Gatfaoui, Noureddine Issaoui, Thierry Roisnel, Houda Marouani, A proton transfer compound template phenylethylamine: synthesis, a collective experimental and theoretical investigations, J. Mol. Struct. 1191 (2019) 183–196, https://doi.org/10.1016/j.molstruc.2019.04.093.

[43] P. Puschnig, M.G. Ramsey, Photoemission tomography: valence band photoemission as a quantitative method for investigating molecular films, Encyclopedia of Interfacial Chemistry (2018) 380–391, https://doi.org/10.1016/B978-0-12-409547-2.13782-5.

[44] Kenichi Fukui, Teijiro Yonezawa, Haruo Shingu, A molecular orbital theory of reactivity in aromatic hydrocarbons, J. Chem. Phys. 20 (1952) 722, https://doi.org/10.1063/1.1700523.

[45] F.B. Asif, F.L.A. Khan, S. Muthu, M. Raja, Computational evaluation on molecular structure (Monomer, Dimer), RDG, ELF, electronic (HOMO-LUMO, MEP) properties, and spectroscopic profiling of 8-Quinolinesulfonamide with molecular docking studies, Comput. Theor. Chem. 1198 (2021), 113169, https://doi.org/10.1016/j.comptc.2021.113169.

[46] S. Muthu Sheryl Cherian Parakkal, Riya Datta, Shine Kadaikunnan, Ghulam Abbas, Solvent-solute polarity, electrophilic, steric effects, reactive sites, themodynamic quantities discussion and biological evaluation of lung cancer antiproliferative activities of spirobrassinin derivatives, J. Mol. Liq. 385 (2023), 122382, https://doi.org/10.1016/j.molliq.2023.122382.

[47] T. Sasitha, Winfred Jebaraj John, design, docking, and DFT investigations of 2,6-bis(3,4-dihydroxyphenyl)-3-phenethylpiperidin-4-one, Heliyon 7 (Issue 2) (2021), E06127, https://doi.org/10.1016/j.heliyon.2021.e06127.

[48] Richard F.W. Bader, A quantum theory of molecular structure and its applications, Chem. Rev. 91 (5) (1991) 893–928, https://doi.org/10.1021/cr00005a013.

[49] F. Akman, N. Issaoui, A.S. Kazachenko, Intermolecular hydrogen bond interactions in the thiourea/water complexes (Thio-$(H_2O)_n$) (n = 1, …, 5): X-ray, DFT, NBO, AIM, and RDG analyses, J. Mol. Model. 26 (161) (2020), https://doi.org/10.1007/s00894-020-04423-3.

[50] R.F.W. Bader, Atoms in molecules, Acc. Chem. Res. 18 (1) (1985) 9–15, https://doi.org/10.1021/ar00109a003.

[51] G. Bharathy, Johanan Christian Prasana, S. Muthu, Irfan Ahmad, Fazilath Basha Asif, A. Saral, S. Aayisha, R. Niranjana devi, Evaluation of electronic and biological interactions between N-[4-(Ethylsulfamoyl)phenyl]acetamide and some polar liquids (IEFPCM solvation model) with Fukui function and molecular docking analysis, J. Mol. Liq. 340 (2021), 117271, https://doi.org/10.1016/j.molliq.2021.117271.

[52] Isabel Rozas, Ibon Alkorta, José Elguero, Behavior of Ylides containing N, O, and C atoms as hydrogen bond acceptors, J. Am. Chem. Soc. 122 (45) (2000) 11154–11161, https://doi.org/10.1021/ja0017864.

[53] Parag Agarwal, Saba Bee, Archana Gupta, Poonam Tandon, V.K. Rastogi, Soni Mishra, Poonam Rawat, Quantum chemical study on influence of intermolecular hydrogen bonding on the geometry, the atomic charges and the vibrational dynamics of 2,6-dichlorobenzonitrile, Spectrochim. Acta Mol. Biomol. Spectrosc. 121 (2014) 464–482, https://doi.org/10.1016/j.saa.2013.10.104.

[54] E.R. Johnson, S. Keinan, P. Mori-Sánchez, J. Contreras-García, A.J. Cohen, W. Yang, Revealing noncovalent interactions, J. Am. Chem. Soc. 132 (2010) 6498–6506, https://doi.org/10.1021/ja100936w.

[55] Chaabane Chiter, Abdelaziz Bouchama, Toma Nardjes Mouas, Hamza Allal, Messaoud Yahiaoui, Warad Ismail, Abdelkader Zarrouk, Amel Djedouani, Synthesis, Crystal structure, spectroscopic and hirshfeld surface analysis, NCI-RDG, DFT computations and antibacterial activity of new asymmetrical azines, J. Mol. Struct. 1217 (2020), 128376, https://doi.org/10.1016/j.molstruc.2020.128376.

[56] Olfa Noureddine, Sofian Gatfaoui, Silvia Antonia Brandan, Abir Sagaama, Houda Marouani, Noureddine Issaoui, Experimental and DFT studies on the molecular structure, spectroscopic properties, and molecular docking of 4-phenylpiperazine-1-ium dihydrogen phosphate, J. Mol. Struct. 1207 (2020), 127762, https://doi.org/10.1016/j.molstruc.2020.127762.

[57] E.R. Johnson, S. Keinan, P. Mori-Sánchez, J. Contreras-García, A.J. Cohen, W. Yang, J. Am. Chem. Soc. 132 (2010) 6498–6506, https://doi.org/10.1021/ja100936w.

[58] T. Lu, qinxue chen, Interaction Region Indicator (IRI): A Very Simple Real Space Function Clearly Revealing Both Chemical Bonds and Weak Interactions, ChemRxiv, 2021, https://doi.org/10.26434/chemrxiv.13591142.v1.

[59] T. Lu, Q. Chen, van der, Waals potential: an important complement to molecular electrostatic potential in studying intermolecular interactions, J. Mol. Model. 26 (11) (2020 Oct 24) 315, https://doi.org/10.1007/s00894-020-04577-0.

[60] D.E. García-Rodríguez, L.H. Mendoza-Huizar, C. Díaz, A DFT study of Cu nanoparticles adsorbed on defective graphene, Appl. Surf. Sci. 412 (2017) 146–151, https://doi.org/10.1016/j.apsusc.2017.03.239.

[61] Heiko Jacobsen. Localized-orbital locator (LOL) profiles of chemical bonding, Can. J. Chem.. 86(7): 695-702, https://doi.org/10.1139/v08-052..

[62] Carlos Silva López, Olalla Nieto Faza, 2 - Overview of the computational methods to assess aromaticity, Aromaticity (2021) 41–71, https://doi.org/10.1016/B978-0-12-822723-7.00002-9.

[63] S. Selvakumari, C. Venkataraju, S. Muthu, Irfan Ahmad, A. Saral, Evaluation of electronic properties in different solvents, spectroscopic exposition (FT-IR, FT-Raman), and molecular docking studies of 5-Chloro-2-hydroxypyridine - insulysin inhibitor, J. Mol. Liq. 341 (2021), 117304, https://doi.org/10.1016/j.molliq.2021.117304.

[64] S. Sundaram, V.N. Vijayakumar, V. Balasubramanian, Electronic and structure conformational analysis (HOMO-LUMO, MEP, NBO, ELF, LOL, AIM) of hydrogen bond binary liquid crystal mixture: DFT/TD-DFT approach, Computational and Theoretical Chemistry 1217 (2022), 113920, https://doi.org/10.1016/j.comptc.2022.113920.

[65] M. Jini Pramila, D. Arul Dhas, I. Hubert Joe, S. Balachandran, Structural, Spectroscopic, Quantum Chemical, RDG, AIM, ELF, Fukui, O–H…N Hydrogen Bonding and NLO Activity of 2-Hydroxy-2-Phenyl Acetophenone Oxime: Experimental and Theoretical Approach, Polycyclic Aromatic Compounds, 2023, https://doi.org/10.1080/10406638.2022.2164016.

[66] Djafri Ahmed, Fouzia Perveen, Nadia Benhalima, Nawel Khelloul, Rachida Rahmani, Ayada Djafri, Abdelkader Chouaih, Mohammed Benali Kanoun, Souraya Goumri-Said, Experimental spectral characterization, Hirshfeld surface analysis, DFT/TD-DFT calculations and docking studies of (2Z,5Z)-5-(4-nitrobenzylidene)-3-N(2-methoxyphenyl)-2-N'(2- methoxyphenylimino) thiazolidin-4-one, Heliyon 6 (Issue 12) (2020), e05754, https://doi.org/10.1016/j.heliyon.2020.e05754.

[67] M. Maria Julie, T. Prabhu, E. Elamuruguporchelvi, Fazilath Basha Asif, S. Muthu, Ahmad Irfan, Structural (monomer and dimer), wavefunctional, NCI analysis in aqueous phase, electronic and excited state properties in different solvent atmosphere of 3-{(E)-[(3,4-dichlorophenyl)imino]methyl} benzene-1,2-diol, J. Mol. Liq. 336 (2021), 116335, https://doi.org/10.1016/j.molliq.2021.116335.

[68] C. Moya Klamt, J. Palomar, A comprehensive comparison of the IEFPCM and SS(V)PE continuum solvation methods with the COSMO approach, J. Chem. Theor. Comput. 11 (2015) 4220–4225, https://doi.org/10.1021/acs.

[69] J. Bai, S. Beyer, D. Trau, 3.331 - Conjugated Polymers for Biosensor Devices, Comprehensive Biomaterials, 2011, pp. 529–556, https://doi.org/10.1016/B978-0-08-055294-1.00121-5.

[70] M. Rana, P. Chowdhury, Effects of hydrogen bonding between pyrrole-2- carboxaldehyde and nearest polar and nonpolar environment, Spectrochim. Acta: Mol. Biomol. 185 (2017) 198–206, https://doi.org/10.1016/j.saa.2017.05.050.

[71] Abdelali Boukaoud, Younes Chiba, Djamel Sebbar, A periodic DFT study of IR spectra of amino acids: an approach toward a better understanding of the N-H and O-H stretching regions, Vib. Spectrosc. 116 (2021), 103280, https://doi.org/10.1016/j.vibspec.2021.103280.

[72] Y.S. Mary, L. Ushakumari, B. Harikumar, et al., FT-IR, FT-Raman and SERS spectra of L-proline, JICS 6 (2009) 138–144, https://doi.org/10.1007/BF03246512.

[73] Y. Sert, Ç. Çırak, F. Ucun, Vibrational analysis of 4-chloro-3-nitrobenzonitrile by quantum chemical calculations, Spectrochim. Acta Mol. Biomol. Spectrosc. 107 (2013 Apr 15) 248–255, https://doi.org/10.1016/j.saa.2013.01.046.
[74] J. Swaminathan, M. Ramalingam, V. Sethuraman, N. Sundaraganesan, S. Sebastian, Vibrational spectroscopic studies and DFT calculations of 4-aminoantipyrine, Spectrochimica Acta. Part A, Molecular and Biomolecular Spectroscopy 73 (4) (2009) 593–600, https://doi.org/10.1016/j.saa.2009.03.009.
[75] B.R. Raajaraman, N.R. Sheela, S. Muthu, Spectroscopic, quantum computational and molecular docking studies on 1-phenylcyclopentane carboxylic acid, Comput. Biol. Chem. 82 (2019) 44–56, https://doi.org/10.1016/j.compbiolchem.2019.05.011.
[76] H.D. Lutz, W. Eckers, H. Haeuseler, OH stretching frequencies of solid hydroxides and of free OH− ions, J. Mol. Struct. 80 (1982) 221–224, https://doi.org/10.1016/0022-2860(82)87236-0.
[77] S. Muthu J, Uma Maheswari, Quantum mechanical study and spectroscopic (FT-IR, FTRaman, 13C, 1H, UV) study, first order hyperpolarizability, NBO analysis, HOMO and LUMO analysis of 4-[(4-aminobenzene) sulfonyl] aniline by ab initio HF and density functional method, Spectrochim. Acta Mol. Biomol. Spectrosc. 92 (2012) 154–163, https://doi.org/10.1016/j.saa.2012.02.056.
[78] Brian C. Smith, The C=O bond, Part III: carboxylic acids, Spectroscopy, Spectroscopy-01-01-2018 33 (1) (2018) 14–20.
[79] Forrest S. Mortimer, Robert B. Blodgett, Farrington Daniels, The infrared spectra of fifteen organic bromides from 500 to 800 Cm-1, J. Am. Chem. Soc. 69 (4) (1947) 822–826, https://doi.org/10.1021/ja01196a022. April 1, 1947.
[80] Chen-Yang Jia, Jing-Yi Li, Hao Ge-Fei, Guang-Fu Yang, A drug-likeness toolbox facilitates ADMET study in drug discovery, Drug Discov. Today 25 (Issue 1) (2020) 248–258, https://doi.org/10.1016/j.drudis.2019.10.014.
[81] R. Thomas, Y.S. Mary, K.S. Resmi, B. Narayana, B.K. Sarojini, G. Vijayakumar, C. Van Alsenoy, Two neoteric pyrazole compounds as potential anti-cancer agents: synthesis, electronic structure, physico-chemical properties and docking analysis, J. Mol. Struct. 1181 (2020) 455–466, https://doi.org/10.1016/j.molstruc.2019.01.003.
[82] A.S. Alwabli, Lead identification against 3C-like protease of SARS-CoV-2 via target-based virtual screening and molecular dynamics simulation, J. Young Pharm. 14 (2) (2022) 179–186, https://doi.org/10.5530/jyp.2022.14.34.
[83] W. Muster, A. Breidenbach, H. Fischer, S. Kirchner, L. Müller, A. Pähler, Computational toxicology in drug development, Drug Discov. Today 13 (7–8) (2008 Apr) 303–310, https://doi.org/10.1016/j.drudis.2007.12.007.
[84] Keith Morris-Schaffer, J. Michael, McCoy, A review of the LD50 and its current role in hazard communication, CS Chem. Health Saf. 28 (1) (2021) 25–33, https://doi.org/10.1021/acs.chas.0c00096. December 21, 2020.
[85] T. Malmfors, A. Teiling, LD50 - its value for the pharmaceutical industry in safety evaluation of drugs, Acta Pharmacol. Toxicol. 52 (Suppl 2) (1983) 229–246, https://doi.org/10.1111/j.1600-0773.1983.tb02692.x.
[86] M. Michael Gromiha, Chapter 5 - protein structure prediction, Protein Bioinformatics (2010) 143–207, https://doi.org/10.1016/B978-8-1312-2297-3.50005-9.
[87] E. Gasteiger, C. Hoogland, A. Gattiker, S. Duvaud, M.R. Wilkins, R.D. Appel, Bairoch A, in: John M. Walker (Ed.), The Proteomics Protocols Handbook, Humana Press, 2005, pp. 571–607. https://web.expasy.org/protscale/.
[88] Sajith Jayasinghe, Kalina Hristova, Stephen H. White, Energetics, stability, and prediction of transmembrane helices11Edited by G. von Heijne, J. Mol. Biol. 312 (Issue 5) (2001) 927–934, https://doi.org/10.1006/jmbi.2001.5008.
[89] Jack Kyte, Russell F. Doolittle, A simple method for displaying the hydropathic character of a protein, J. Mol. Biol. 157 (Issue 1) (1982) 105–132, https://doi.org/10.1016/0022-2836(82)90515-0.
[90] M.S. Boguski, M. Freeman, N.A. Elshourbagy, J.M. Taylor, J.I. Gordon, On computer-assisted analysis of biological sequences: proline punctuation, consensus sequences, and apolipoprotein repeats, JLR (J. Lipid Res.) 27 (Issue 10) (1990) 1011–1034, https://doi.org/10.1016/S0022-2275(20)38761-7.
[91] R.A. Laskowski, E.G. Hutchinson, A.D. Michie, A.C. Wallace, M.L. Jones, J.M. Thornton, PDBsum: a Web-based database of summaries and analyses of all PDB structures, Trends Biochem. Sci. 22 (12) (1997 Dec) 488–490, https://doi.org/10.1016/s0968-0004(97)01140-7.
[92] Marco Wiltgen, Algorithms for structure comparison and analysis: homology modelling of proteins, Encyclopedia of Bioinformatics and Computational Biology (2019) 38–61, https://doi.org/10.1016/B978-0-12-809633-8.20484-6.
[93] Supratim Choudhuri, Chapter 8 - Additional Bioinformatic Analyses Involving Protein Sequences**The opinions expressed in this chapter are the author's own and they do not necessarily reflect the opinions of the FDA, the DHHS, or the Federal Government, Bioinformatics for Beginners (2014) 183–207, https://doi.org/10.1016/B978-0-12-410471-6.00008-6.
[94] https://www.niaid.nih.gov/diseases-conditions/hepatitis.
[95] H.M. Berman, J. Westbrook, Z. Feng, G. Gilliland, T.N. Bhat, H. Weissig, I.N. Shindyalov, P.E. Bourne, The protein data bank, Nucleic Acids Res. 28 (2000) 235–242, https://doi.org/10.1093/nar/28.1.235.
[96] R. Sravanthi, S. Mahalakshmi, V. Vetrivelan, Irfan Ahmad, S. Muthu, Absorption wavelength (TD-DFT) and adsorption of metal chalcogen clusters with methyl nicotinate: structural, electronic, IRI, SERS, pharmacological and antiviral studies (HIV and omicron), Heliyon 9 (Issue 5) (2023), e16066, https://doi.org/10.1016/j.heliyon.2023.e16066.
[97] Vibha Vinayakumar Bhat, P.R. Chetana, Mohan A. Dhale, Sreejit Soman, Synthesis, characterization, in vitro biological evaluation and molecular docking studies of newly synthesized mononuclear lanthanum(III) complexes of N,N'-bis(2-aminoethyl)oxamide and phenanthroline bases, J. Mol. Struct. 1270 (2022), 133903, https://doi.org/10.1016/j.molstruc.2022.133903.
[98] T. Eichhorn, F. Kolbe, S. Mišić, D. Dimić, I. Morgan, M. Saoud, D. Milenković, Z. Marković, T. Rüffer, J. Dimitrić Marković, et al., Synthesis, crystallographic structure, theoretical analysis, molecular docking studies, and biological activity evaluation of binuclear Ru(II)-1-Naphthylhydrazine complex, Int. J. Mol. Sci. 24 (1) (2023) 689, https://doi.org/10.3390/ijms24010689.
[99] Umar Faruq Chowdhury, Abdullah Al Saba, Abu Sufian Sufi, Akib Mahmud Khan, Ishrat Sharmin, Aziza Sultana, Md Ohedul Islam, Subtractive proteomics approach to Unravel the druggable proteins of the emerging pathogen Waddlia chondrophila and drug repositioning on its MurB protein, Heliyon 7 (Issue 6) (2021), e07320, https://doi.org/10.1016/j.heliyon.2021.e07320.
[100] Olfa Noureddine, Sofian Gatfaoui, Silvia Antonia Brandán, Houda Marouani, Noureddine Issaoui, Structural, docking and spectroscopic studies of a new piperazine derivative, 1-Phenylpiperazine-1,4-diium bis(hydrogen sulfate), J. Mol. Struct. 1202 (2020), 127351, https://doi.org/10.1016/j.molstruc.2019.127351.